UC San Diego
UC San Diego Electronic Theses and Dissertations

Title

Temporal and spatial study of drying of suspension and solution droplets for tablets coating purposes

Permalink

https://escholarship.org/uc/item/7rq4616p

Author

Sartori Velasco, Silvana

Publication Date

2010

Peer reviewed|Thesis/dissertation

UNIVERSITY OF CALIFORNIA, SAN DIEGO

**Temporal and Spatial Study of Drying of Suspension and Solution
Droplets for Tablets Coating Purposes**

A thesis submitted in partial satisfaction of the
requirements for the degree
Master of Science

in

Engineering Sciences (Aerospace Engineering)

by

Silvana Sartori Velasco

Committee in charge:

Professor Juan C. Lasheras, Chair
Professor Alison Marsden
Professor Juan Carlos Del Álamo

2010

The thesis of Silvana Sartori Velasco is approved, and it is acceptable in quality and form for publication on microfilm and electronically:

_____

_____

_____
                                          Chair

University of California, San Diego

2010

TABLE OF CONTENTS

NOMENCLATURE

Symbols

C_p Specific Heat at Constant Pressure (J/kg K)

D_{BD} Mass Diffusion Constant (m^2/s)

k_g Gas Thermal Conductivity (W/K m)

L Distance from atomizer to tablet (m)

L_v Specific Latent heat of vaporization (kJ/kg)

Subscripts

B Boiling

b Bubble

f Final

g Gas

i Inner

l Liquid

p Precipitate

s Surface

sat Saturation

$solu$ Solute

$solv$ Solvent

LIST OF FIGURES

ACKNOWLEDGEMENTS

I must start by thanking Professor Juan Lasheras who accepted to be my advisor. He gave me the opportunity to learn what research is, gave me great advice professionally as well as personally. He has been my mentor, and I believe I am a more complete person after these 2 years working with him. I have learnt that research is hard enough on its own, let alone if dealing with aside issues. Thanks a lot.

Without the help of Professor Amable Liñán I would have been clueless at the the beginning of my research. He has the capability to shed light to scientific problems in such a way that one sees them as easy, no matter how hard the problem is.

As for students, I need to truly thank Jorge Arrieta and Pablo Martínez Legazpi. They both inspired me to keep working and helped me in various stages of the thesis. The two of them have became really good friends, and I thank them for being also part of my life. Las vueltas que da la vida!

During these two years spent in San Diego, and at UCSD, I have met many people, made really good friends, found fantastic classmates and office mates and met random amazing people. I need to thank all of them for how fantastic people they are, for how, in some way or another, have made this stay in San Diego and at UCSD unforgettable. These two years, and the outcome of it, this thesis, has been possible thank to every friend who has supported me on this journey, who had to deal with my stress (not that many times though), my research-related or unrelated problems. And these friends are (not any specific order): Baldo, Katie, Effie, Bego, Manu, Javi (my graduate mentor y hombro en el que llorar!), Jessica, Dib, Mike (good thesis tips!), Kevin, Eric A., Marie, Lili, Kelly, Yulia, Sun Hwa, Claudia, Marco, Dave, Ali, Ahsan, Jorge, Pablo, Dani, Celso, David, Viktoria (great talks!), Kaitlyn (best roomate ever!), and many more. Please do not take it personal if your name is not here! I was running out of time! I need to especially mention Effie and Katie. You are great friends and you have proved it to me countless times! I had the greatest times with you girls and will never forget all of your advices.

VITA

2004	Undergraduate Researcher, Von Karman Institute for Fluid Dynamics, Belgium
2007	Ingeniero Aeronáutico (Specialization in Space Vehicles and Missiles), Universidad Politécnica de Madrid, Spain
2008	Systems Engineer, A400M Project, Military Transport Aircraft Division (EADS), Spain
2008-2010	Graduate Teaching Assistant, University of California, San Diego
2010	Master of Science, Mechanical and Aerospace Engineering, University of California, San Diego

PUBLICATIONS

Sartori, S., Liñán, A., Lasheras, J. C., *An evaporation model of colloidal suspension droplets* Oral Presentantion. 62nd Annual Meeting of the American Physical Society's Division of Fluid Dynamics. November, 2009

ABSTRACT OF THE THESIS

Temporal and Spatial Study of Drying of Suspension and Solution Droplets for Tablets Coating Purposes

by

Silvana Sartori Velasco

Master of Science in Engineering Sciences (Aerospace Engineering)

University of California, San Diego, 2010

Professor Juan C. Lasheras, Chair

Suspensions or solutions of polymers are widely used in the pharmaceutical industry to coat tablets with different agents. These allow controlling the rate at which the drug is delivered, taste or appearance. The coating is performed by spraying and drying the tablets at moderate temperatures. The spreading of the coating on the pills surface depends on the droplet Webber and Reynolds numbers, angle of impact, but especially on the rheological properties of the drop.

We present simplified models for the evaporation of suspension and solution droplets in a hot air environment with temperatures substantially lower than the boiling temperature of the carrier fluid. As the liquid vaporizes from the surface in the solution case, the solution becomes more concentrated, until reaching its saturation point. After saturation, precipitation occurs uniformly within the drop. As the surface regresses, a compacting front formed by the solid precipitate at its maximum packing density advances into the drop, while more solute continues precipitating uniformly. The porous shell grows faster than in the suspension case, due to the double effect of surface regression and precipitation.

Chapter 1

Introduction

1.1 General Introduction

Film coatings are often used to enhance pharmaceutical tablet products. Tablet film coatings can provide many benefits including: improved appearance, added functionality (e.g., sustained release, delayed release or coatings with active ingredients), brand identity, dose strength identification, improved tablet taste, improved mechanical strength for handling during production packaging, reduce worker exposure (e.g., when dispensing in a pharmacy or hospital setting). There is also potential to improve chemical stability by separation of incompatible ingredients into layers. Improvements in stability can be significant for maintaining drug potency, reducing or masking potential color changes in the tablet core, or reducing the development of odors due to chemical reactions. However, coating ingredients may also cause instability of the tablet composition. Hence, a good understanding of the coating process will lead to a precise control of its conditions, critical for successful product development.

1.2 Relevant Physical Processes

Tablet coating has evolved throughout history from sugar based coatings, to solvent based polymeric or aqueous based polymeric film coatings. Equipment preferences have also changed from non-perforated pans to partially or fully perforated pans. Coating application has also drastically improved from ladling of sugar coatings
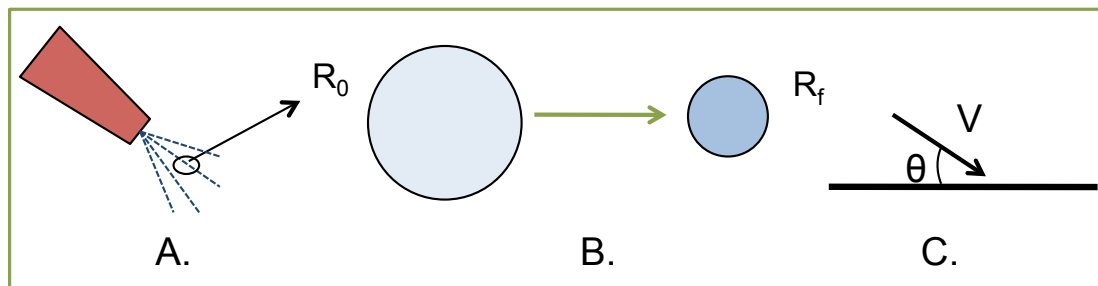
Figure 1.1: The three main physical processes of interest to study. A. Atomization of the fluid. B. Vaporization and composition change of the drops. C. Impact of the drops onto the tablet

to films applied with modern pneumatic or coaxial air blast spray guns.

The application of coating material to the tablets is carried out in a complex process that includes 4 key steps: spray atomization, droplet transport, droplet impact and tablet drying, and tablet mixing. A schematic of the three main physical processes involved in tablet coating is shown in figure 1.1. Mathematical and physical modeling of these three aspects of tablet film coating are important and may reach impact on the economics of pharmaceutical commercialization, potentially reducing both cost and time to market. In the last step of the process, a batch may be rejected if process conditions are poorly selected or controlled. Tablets with surface defects may be removed from the batch after a complete visual quality inspection; however, this added step expensive is time consuming and should be avoided.

Although the coating process is the above described, the techniques and standard equipments to obtain these coatings may differ. Coating may be performed in batches, where a fluidized bed of tablets is sprayed either from the top, the bottom or tangentially (figure 1.2) in batches; in a continuous manner (figure 1.3) equally spraying from the top or from the bottom. Pan coating is however the type of coating that we will be focusing on in this project (figure 1.4): a rotating drum with a batch of tablets is sprayed from either the center or the surface of the drum; a drying gas is injected either in the same direction of the spray or the opposite direction.

Summarized hereafter are the three main steps of tablet coating.

First, the coating formulation is atomized into small droplets (sketch A of figure 1.1). This is done by using two-fluid coaxial atomizers in which the liquid

**Batch fluid bed
coating
Top Spray**

**Batch fluid bed coating
Bottom Spray
(Wurster Coating)**

**Batch fluid bed coating
Tangential Spray**
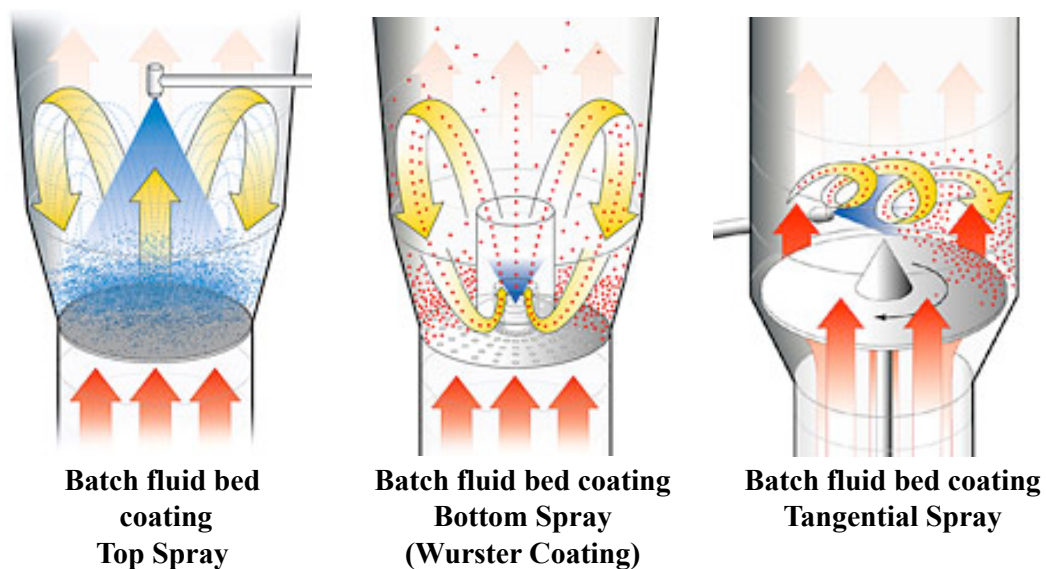
Figure 1.2: Particle Coating and Encapsulation: Batch.

Top Spray

Bottom Spray

Coating in a continuous fluidized bed
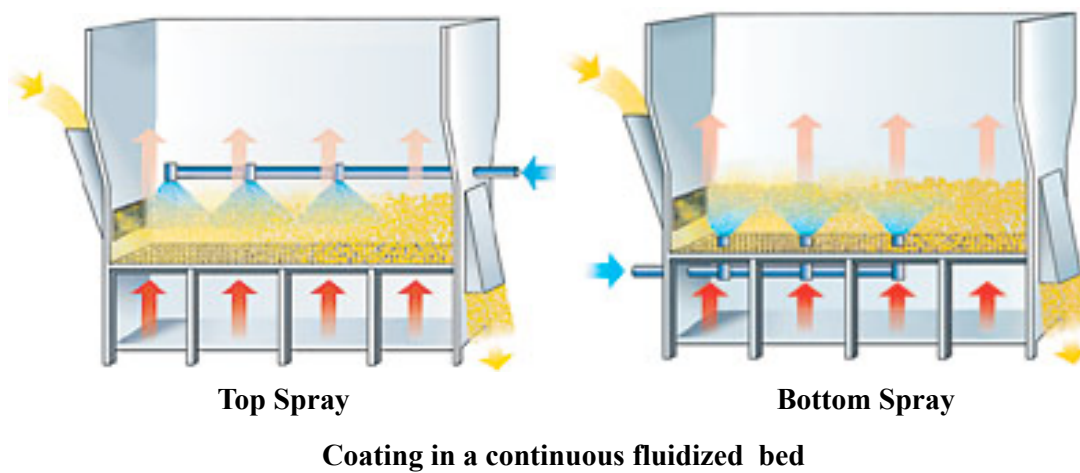
Figure 1.3: Particle Coating and Encapsulation: Continuous
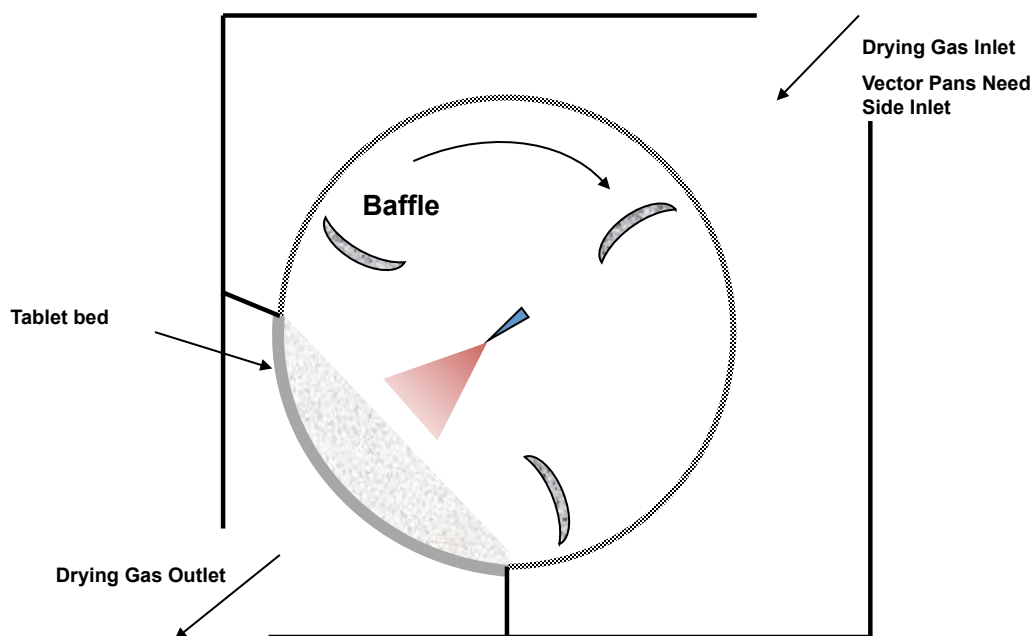
Figure 1.4: Particle Coating and Encapsulation: Pan Coating

formulation is injected through the inner nozzle at low speed and a process gas, typically air, is injected through the outer nozzle at very high speed. The atomizing gas exerts normal and shear forces on the liquid jet, producing instabilities at the liquid/air interface, which will evolve into the break-up of the liquid jet into droplets (see figure 1.5). This type of atomizer allows independent control of the liquid mass flow rate and droplet size. This is because the liquid speed at the nozzle is low and the break-up process that determines the droplet size is a function of the velocity difference between the two fluids which can be modified by changing the gas speed, keeping constant the liquid flow rate.

The second step in the process is the transport of the liquid droplets onto the tablets surface (sketch B of figure 1.1). The droplets move under the velocity transferred to them by the atomizing gas and are partially dried by a secondary flow of hot dry gas that is introduced with negligible momentum into the process chamber, so as not to disturb the droplet motion. This secondary gas flow provides the heat needed to dry the solvent used in the coating formulation while keeping a sensitive balance between too little drying (droplets hitting the tablets with too much solvent)
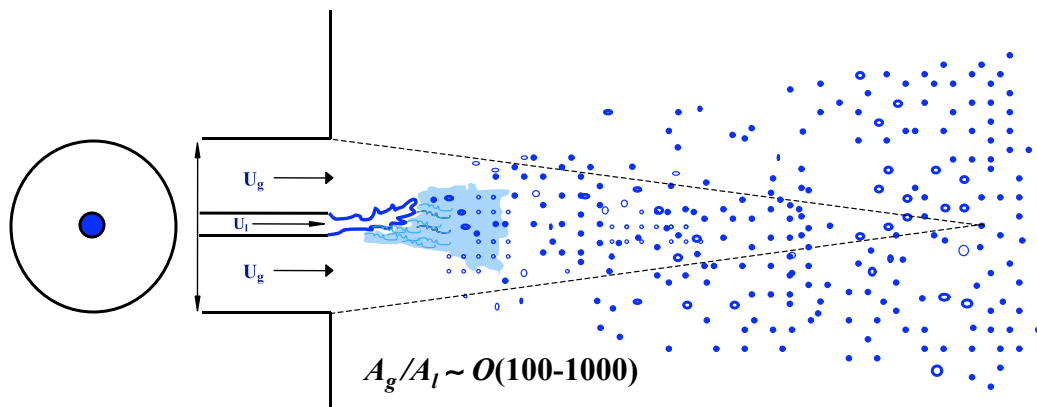
Figure 1.5: Scheme of a coaxial atomizer

and too much drying (droplets drying out entirely during their transport).

The third step is the impact and spreading of the droplets onto the tablets (sketch C of figure 1.1). The droplets spray hits the tablets at or near the surface of the bed. By rotating the drum, the tablets in the bed will tumble, allowing the individual tablets to form a continuous coating film due to the spreading and following drying of the small coating droplets impacting at all times during the process. This last aspect forms the third elementary process that determines the success of the operation. For the droplet spreading on the individual tablets to lead to a uniform film coating, the tablets need to be adequately mixed in their recirculating porous bed.

Small droplets can dry too much before impacting the tablet and lead to reduced coating efficiency, or they may fail to coalesce on the tablet surface, producing a non smooth, non continuous porous film. While droplets that are too large, on the other hand, may have reduced solvent evaporation and lead to over-wetting. This causes coating defects, such as sticking marks if tablets have been stuck to each other or rough coatings due to erosion of the tablet core components.

The vaporization process is then a key part of the tablet film coating process. It is therefore of great importance to develop physics-based vaporization models that can predict changes in droplet size and composition as a function of fluid properties, ambient conditions and atomization conditions. These models can play an important role in the design of the process, including selection of equipment and process param-

eters, and in the optimization and control at all different levels: lab, pilot and full scale.

The spreading of the coating on the pills surface depends on the droplet Webber and Reynolds numbers, angle of impact, but more importantly on the rheological properties of the drop (viscosity, surface tension), and on the non internal uniformities of the droplets. And, as already mentioned before, these factors will cause heterogeneity, splashing and porosity of the coated layer. The following chapters will explain and develop models of the evaporation of droplets of two types of coating fluids used in the pharmaceutical industry, when immersed in a hot air environment with temperatures substantially lower than the solvent or carrier fluid boiling temperature.

Chapter 2

Literature Review

2.1   Introduction

We are interested in modeling the time and spatial evolution of the size and composition of a single droplet of either a colloidal suspension or a solution, of initial diameter D_0 ranging from 20 to 100 μm, traveling with a jet of air (atomization air) with initial speed V_0 The drop is ejected at a distance from the point of impact (the tablets bed) L. The surrounding air is considered to be at uniform temperature T_∞ throughout the distance traveled by the drop. We let the droplet travel, while decreasing its speed as the jet of air does, until it impacts the tablet.

Drops of colloidal suspension are composed of spherical micron-size solid particles (typically TiO_2 [1]) suspended in a carrier liquid, typically water or acetone. When the solid can be dissolved within the solvent, the mixtures are called solutions. The vast majority of solutions used in the pharmaceutical industry for tablet coating are either acetone-based or water-based solutions , with a mixture of polymers as solute [2, 3, 4]. While the main solvent is either acetone or water, a small percentage of the other fluid can be found in the mixture. But since it is a very small percentage of the total drop mass (a sample composition would be:s 90% acetone, 5% water, 5% polymers [5]), the solution is mainly composed of a single solvent and a single solute , each of them with rheological properties (density, surface tension, viscosity) calculated as the weighted average of the solvent and solute components properties respectively.

2.2   Spray Atomization

Spray atomization has been widely used for decades in the field of combustion [7, 8]; fuel injection in automobile and turbo jet engines, or rocket engines are some of the applications of sprays in combustion. Lately, the use of spray atomization is being spread; the production of polymeric hollow spherical particles [9, 10], by spraying very fine droplets of a solution or suspension of a polymer into a carrier fluid and letting dry these droplets until obtaining spherical particles with a certain morphology or porosity; the production of cosmetic powders is performed spraying and drying different types of suspensions or solutions.

As mentioned in the introduction, spray of the coating solution is done by means of a coaxial atomizer. The liquid jet exits through the interior tube, while the coaxial tube carries the gas at very high speed. The atomization occurs when instabilities are induced in the liquid jet by the high speed gas jet [11], breaking up the liquid jet. First, the liquid breaks into tongues of liquid away from the jet (Kevin-Helmholtz instability), pushed towards the high speed coaxial jet. As a low-speed tongue of liquid is inserted in the gas phase, the air jet will accelerate the tongue, occurring a secondary instability (Rayleigh-Taylor instability), which will further break up the tongues of fluid into smaller and smaller droplets.

The primary as well as secondary instabilities induced by a high-speed air stream have been extensively studied [12, 13] and modeled for Newtonian fluids. However, very little [14] is known about atomization of non-Newtonian fluids. The Weber and Reynolds numbers are of relevance in this process, since they contain information about the liquid surface tension as well as viscosity, two important rheological properties for non-Newtonian fluids.

Air-blast atomization of viscous non-Newtonian liquids using a co-axial twin-fluid atomizer was studied by Mansour et al [14]; their study showed that becaue the normal stresses developed in viscoelastic materials are much higher than their associated shear stresses, these large normal stresses appear to be the most important rheological mechanism that inhibits breakup.

Aliseda et al [16] took a step further, not only studying the liquid break up and spray atomization of non-Newtonian fluids, but also estimating the Sauted Mean

Diameter (a probabilistic weighed averaged diameter) of the droplets in terms of the fluid rheological properties, as well as the distance from the atomizer nozzle and the atomization parameters (speeds, flow rates, ...). The predictions of the mathematical model matched very well with experiments that Aliseda et al performed.

2.3   Droplet Vaporization

In combustion, after atomizing and obtaining small droplets of liquid, and before burning the droplets of fuel, one also has to deal with the vaporization process occurring. Being immersed these drops in very hot reacting environments, vaporization is very likely to happen, before the combustion reaction occurs.

The vaporization of a single pure liquid drop in a hot quiescent ambient is a well known process thanks to the work of the combustion community. Mathematical models as well as experimental studies [17, 18] on the droplet combustion and vaporization have been developed over the years. The simultaneous solution of the mass, species and energy conservation equations with their corresponding simplifications lead to the well known "d-square Law", which states that during evaporation of a droplet in a quiescent environment, the squared of the diameter of the droplet decreases linearly with time [7, 19].

The experimental and analytical studies of the vaporization and combustion processes of metal, coal slurry droplets [20], water-in-oil emulsion studied by Lasheras [] and multicomponent fuel droplets by Law [21] have broadened the field of drop vaporization to more complex drop structures, including multicomponent, suspension drops, and drops immersed in a different fluid.

2.3.1   Multicomponent Droplet Vaporization

A model for evaporation of a multicomponent droplet near its boiling temperature was proposed by Newbold and Amundson [23]. Although the increase of diffusive mass transfer due to the Stefan flow (bulk) from the droplet, was known to play an important role in single component droplet vaporization, it plays an even greater role in multicomponent droplets, describing more accurately the evaporation

taking place near the boiling point, and therefore including it in this new model.

The relevant limiting case for heat and mass transport within a droplet of a not so viscous mixture occurs when the droplet temperature and composition are spatially uniform, but not temporally, due to the fast internal circulation. To have rapid internal mixing, a large air velocity relative to the droplet is needed. The shear stresses at the surface due to this high velocity create internal vortices that mixes the droplet content. If this is the case the relative Reynolds number must be greater than 300, thus the droplet is not vaporizing in a quiescent environment and the "d-square Law" should not be applied. However, one does not need to have a natural or forced convection to obtain these vortices. Law claims that a violent atomization process can infer internal circulation in the droplets and persist throughout the droplet life time.

In Law's model, the most volatile components are continuously brought to the droplet surface where they will preferentially vaporize. The main assumptions and simplifications included in the model proposed by C. K. Law [24] for vaporization of multicomponent droplets, are very similar to the ones made for the model proposed in this thesis.

- Spherically symmetric evaporation of the droplet.

- Vaporization is a diffusion-driven process, that is, due to the diffusion of the vapor in the gas phase (air), more solvent can vaporize at the surface of the droplet.

- Uniform ambient temperature.

- Zero-concentration of the species contained in the droplet far away from it $(Y_{i,\infty} = 0)$

- The species concentration and the temperature within the droplet become uniform at a rate, which is much faster than the rate at which the average droplet properties change but still shorter than the gas-phase heat and mass transfer rates.

  Existing experimental evidence shows that internal circulation, producing a rapid internal mixing of the different components, is the rate-controlling process,

instead of diffusion. It can be produced during the initial atomization process but also by means of forced or natural convection. In this case, the violent atomization process that takes place prior to vaporization will produce the needed internal circulation.

2.3.2 Drying of Suspension and/or Solution Droplets

Most of the models, despite the complexity of the heat and mass transfer model, found in the literature divide the drying process into two distinct phases. One, in which the droplet shrinks because of the vaporization of the solvent, and the second one in which a dry porous crust is formed either from the precipitated solute on a solution drop, or from the agglomeration of the suspended particles. Once the porous crust is formed, the droplet size is claimed to remain constant during this second phase; its voids are filled with air through which the liquid vapor diffuses toward the surface. The wet core is then the one decreasing in size, regressing as the liquid inside it vaporizes and diffuses away through the pores, while the outer shell remains intact.

Unlike most of the models where the critical point where the drop stops shrinking is the saturation point, Werner et al [27] developed an effective diffusion model that was used to predict ideal shrinkage until a critical $(T - T_g)$ (where T_g is the glass transition temperature of the polymer) is reached where the surface area of the droplet becomes fixed and the skin grows towards the droplet center as a regressing interface (see figure 2.1 and 2.2) However, the model was developed considering Maltodextrin as the polymer, which has a very low saturation concentration of approximately $17\% \, wt$. Despite the fact that even at $40\% \, wt$ on Werner's previous work [28] they noted that the solutions were viscous and able to flow. In this most recent paper, Werner et al claim that the conditions leading to the state of dry skin and to the definition of the radius at which it forms, remained unclear, proposing now a new model based on the glass transition temperature. It also has to be noted that the ambient temperature at which the drying is occurring is about $78 \, ^oC$ which is higher than the drying temperatures used on tablet coating.

Mezhericher et al [29] claimed to have developed an advanced theoretical model
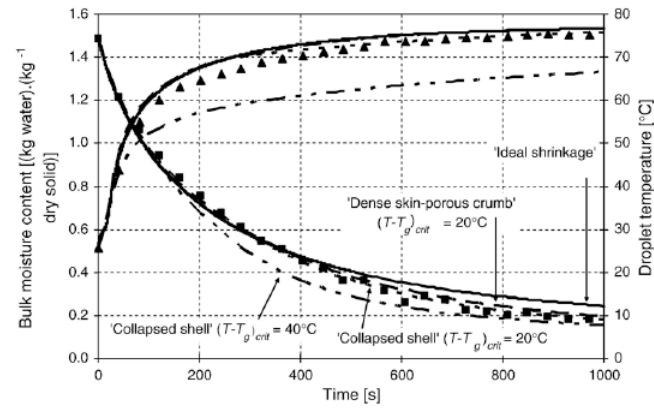
Fig. 2. Effect of $(T-T_g)_{crit}$ value and the variable density calculation schemes on the droplet temperature on the moisture content predictions for 40 wt.% maltodextrin DE5 droplets at 78 °C: ■ experimental moisture content; ▲ experimental temperature; —— 'Ideal shrinkage' model predictions; – – 'Collapsed shell', $(T-T_g)_{crit}$=20 °C predictions; ▬ - - ▬ 'Collapsed shell', $(T-T_g)_{crit}$=40 °C predictions; ▬ ▬ 'Dense skin-porous crumb', $(T-T_g)_{crit}$=20 °C predictions.

Figure 2.1: Effect of $(T - T_g)$ on the droplet moisture content and temperature
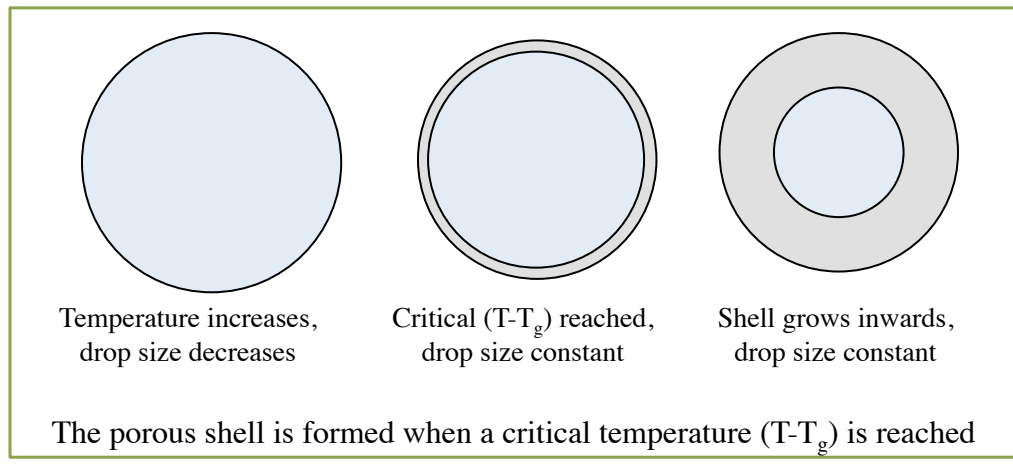
Figure 2.2: Werner's vaporization model using glass transition temperature of the polymer

that can describe more realistically the drying process of single suspension or solution droplets. The model contemplates a first stage of initial heating-up of the drop, where the "d-square Law" still holds, as well as a temperature profile within the drop, heat absorption by the dried crust, crust porosity and temperature dependence on droplet physical properties. During the second stage, when saturation is reached, the droplet is treated as a wet particle, having a wet core surrounded by a porous crust. Although their model predictions fit well the experimental data, the solutions and suspensions used have a very high solid loading, as well as large size droplets and high ambient temperature, while during the pills coating process, the atomization of a very dilute solution produces smaller droplets and the drying air temperature is around $25-60\,^oC$, instead of $30-95\,^oC$.

Computational models may remove some of the simplifications needed when developing an analytical model, as done by Dalmaz et al [30]. The model is slightly different than the majority in terms of the stages. The first stage is characterized by having a wet core, with the solid particles in it, and a pure liquid shell (free water) whose interface regresses as water is evaporated. During the second stage, the same inner wet core with the solid particles is surrounded by a dry shell, a porous solid shell. The computational model is able to predict the drop size and temperature time evolution, matching the experimental data. However, droplets initial radii range from 0.8 to 0.9 mm, which are drop sizes that the atomizer cannot generate.

The work of Yarin et al [31] in vaporization of acoustically levitated suspension drops showed mathematically and experimentally that during the first stage the "d-square Law" still holds during vaporization, while during the second stage the drop size remains constant. Despite the high solid mass fraction and the large sizes (up to 10 mm), their experimental data on temporal evolution of droplet size will be used to compare it with the results from the vaporization model for suspension droplets proposed in this thesis.

As a summary, a large percentage of the models and experiments found in the literature [32] deal with droplets one or two orders of magnitude greater than the case we are interested in ($0.9\,mm - 10\,mm$), of mixtures with a high initial mass fraction of solute or solid particles ($20\,\% - 40\,\%$) and small saturation mass fraction ($17\,\%$), drying in a large range of temperatures ($30\,^oC - 200\,^oC$).

The conditions encountered during the coating process of pharmacological tablets are the following: droplet diameters range from 20 to 100 μm, the drying air temperature range from 25 ^oC to 60 ^oC, and the initial solute mass fraction of the solution ranges from 5 % wt to 15 % wt.

As mentioned at the beginning of this section, most of the models describe the second stage as the formation of a dry and porous crust [37, 38]. However,if this is the case, especially for suspension droplets, it implies that the solid particles remain tightly close to each other, with voids filled with gas in between the spherical particles. Due to the low drying temperatures considered here, there will be no dry crust. This will only happen in combustion or if the drop is at very high temperature. To illustrate it with an example, to compact a ball of sand at low temperatures, a liquid is needed to keep the sand grains together. Surface tension is the cohesive force that will keep the grains compacted. If the sand is completely dry, the grains will not stick together and the structure will fall apart.

2.4   Impact of Droplets

The impact of a liquid droplet on a solid surface is a very common problem in nature and industry. Despite the considerable amount of effort devoted to droplet impact over the past century, there has been little attention directed towards pharmaceutical coating processes by which a thin coating is applied on tablets through a spray. Solid and liquid surface impacts have been studied which has prompted two reviews on the subject, [39, 40].

When a liquid drop orthogonally impacts a solid substrate, the drop may deposit into a thin disk, disintegrate into secondary droplets, or recede and possible bounce. When inertia is negligible the drop will deposit gently over the surface until equilibrium is reached. This equilibrium is a function of the solid/liquid/gas contact point commonly defined by the contact angle, θ (see figure 2.3).

If the contact angle is at a minimum ($\theta = 0$), the drop will spread indefinitely into a thin film, potentially reaching molecular. If $\theta > 0$, the drop will attain equilibrium once balance is reached between gravity, capillarity, and viscosity in a time of order of seconds. If the drop approached the substrate with sufficient kinetic energy,
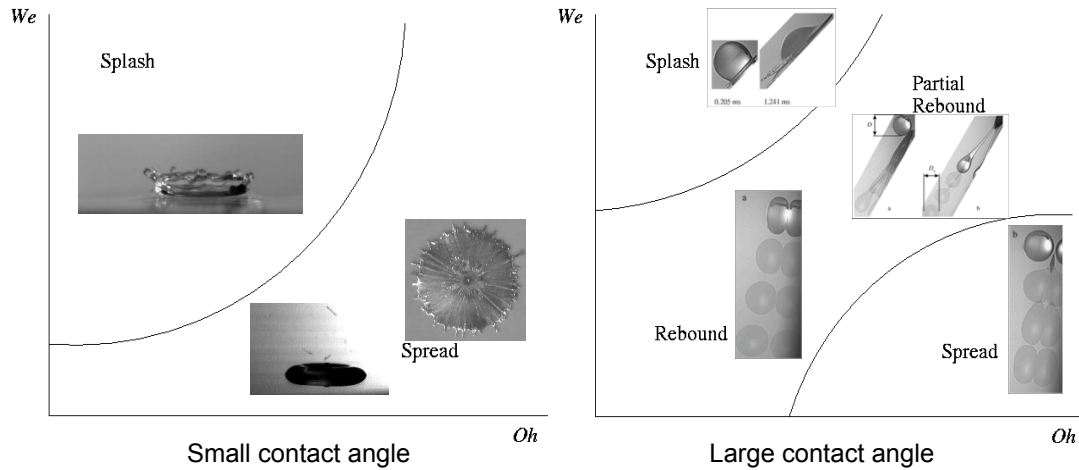
Figure 2.3: Types of droplet impact onto a solid surface for small (left) and large (right) contact angles

then the balance is complicated by the addition of inertia. When the surface/liquid combination has a high contact angle ($\theta > 90^oC$) at equilibrium, then inertia will act to maintain excess surface energy upon impact and may partially recede the drop and even completely lift the drop off the surface. If the substrate is roughened, the drop can splash upon impact.

Bolleddulla et al [41] conducted a systematic study of droplet impact with both Newtonian fluids with high viscosity and colloidal suspensions. They performed experiments on droplets impact and compared them with different available models and theoretical studies on droplet impact. They demonstrated that at viscosities and Weber numbers ranges of $\mu = 10 - 100\,cP$ and $We = 1 - 300$ respectively, the drop impact resulted in spreading avoiding splash and rebound, with a minimal recession of the spreading diameter. The role of viscosity observed with and without colloids is thought to explain the repression of splashing and rebounding. In experiments with colloidal suspensions at $We \sim 30$, the height of the rim, when the drop spreads after impact, was found to increase linearly after the apex of the drop sinks below the rim as spreading is arrested.

In this paper they confirm previous studies that during the initial stages of impact under certain conditions, the spreading diameter is insensitive to wettability, observing also reasonable agreement with two existing impact models. The models

provided by [42] and [43] are still valid as a robust model for first order approximations.

2.5   Purpose of the Thesis

As already introduced in the first section of this chapter, in this research we are interested in modeling the time and spatial evolution of the size and composition of a single droplet of either a colloidal suspension or a solution, to be able to predict the formation of a fully compacted, but wetted, shell as well as the time at which that shell begins to form and its time evolution. This is the reason why many (although well justified) simplifications were made in the heat and mass transfer equations in an attempt to focus on the compactation and/or precipitation of the solute. The simplifications and assumptions to obtain the vaporization models are collected in the following figure 2.4.

The estimated time needed for the drop to reach its terminal speed relative to the jet is very small compared to the estimated vaporization time. Hence, no convection term is included, since the relative Reynolds number is small. This assumption seems to invalidate the rapid internal mixing assumption from the multicomponent droplet model proposed by C. K. Law [24], which needed of a high shear stress at the droplet surface produced by the air flow around it. However, Law recalled that internal circulation can be achieved at the initial atomization stage, if it is sufficiently violent. On a coaxial atomizer, the gas speeds are extremely high compared to the liquid speeds. The liquid stream is then sped up and broken-up into droplets. This type of atomization can be considered a violent atomization which will infer an internal circulation to the droplets that will last throughout their life time.

We propose two vaporization models. The model for a colloidal suspension droplet is a one-stage process, while for a solution drop the vaporization is divided into two stages: a first stage, during which the drop is a multi-component drop with the solid diluted, and the second stage, during which the solute begins to precipitate.

As shown in figure 2.5, vaporization of the solvent is a diffusion-driven process that occurs at the surface. Because the surrounding air is dry of solvent vapor, the vapor being tansformed at the surface will diffuse away from the drop surface allowing

ASSUMPTIONS AND SIMPLIFICATIONS	
FROM PREVIOUS MODELS	**FOR SUSPENSION AND SOLUTION DROPS**
• Spherically symmetric evaporation of the droplet • Vaporization is a diffusion-driven process. Due to the diffusion of the vapor in the gas phase (air), more solvent can vaporize at the surface of the droplet • Uniform ambient temperature • Zero-concentration of the species contained in the droplet far away from it ($Y_{I,\infty}=0$) • The species concentration and the temperature within the droplet become uniform at a rate much faster than the rate at which the average droplet properties change, but still shorter than the gas-phase heat and mass transfer rates • Rapid internal mixing	• The liquid-phase species concentration will vary temporally, since the solute remains within the drop while the solvent vaporizes, until the droplet reaches saturation conditions. Then precipitation of the solute will begin • When the solute reaches its critical or saturation point, it precipitates in form of spherical particles • Precipitation of the solute occurs uniformly throughout the droplet • Negligible Brownian diffusion: the precipitated solid particles have such size that the time for the particles to diffuse within the drop is much larger than the estimated time required to vaporize all the solvent. Therefore, we can assume what we call "frozen limit". The particles are uniformly distributed and do not move while vaporization is occurring

Figure 2.4: Assumptions and simplifications to develop the vaporization models of this research
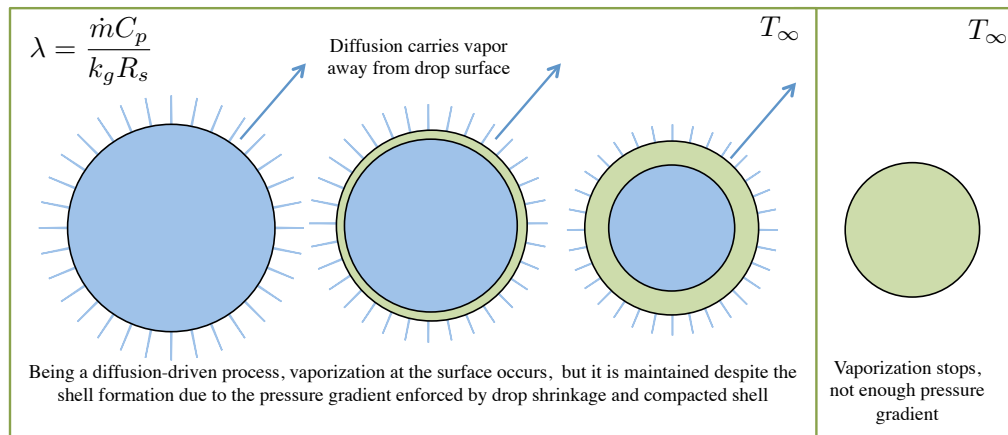
Figure 2.5: Suggested process of droplet vaporization

more liquid to evaporate. Once a wet shell is formed, the solids within the drop are maximally compacted at the surface as it regresses and the solvent continuously vaporizes at the surface. However, as the shell thickness keeps growing, the pressure gradient across the layer will decrease, and once the droplet is fully compacted, the pressure gradient will not be enough to continue vaporization, finalizing the process.

Chapter 3

Vaporization Model

3.1   Vaporization of a Pure Liquid Droplet

As mentioned in chapter 2, most of the work on droplet vaporization has been done by the combustion community. Combustion, burning and vaporization of pure liquid, multi-component or metal slurry droplets have exhaustively been studied, proposing theoretical models and validating them with experiments under many conditions.

Being the goal of this research to model the vaporization process of solution and suspension droplets, I will briefly summarize here the vaporization of a single pure liquid droplet.

A liquid drop of initial radius R_0 is surrounded by a stream of dry air, with small velocity U relative to the air, at a temperature T_∞. Due to the droplet composition, the ambient temperature and the parameters here below explained, no reaction will occur, hence no combustion, but only vaporization will take place. At any given time t the drop surface will be at $R_s(t)$

The droplet response will depend on various dimensionless numbers, such as:

- Peclet number, defined as the ratio of the drop inertia to its thermal diffusivity
  $Pe = \frac{UR_s}{\alpha}$

- Prandtl number, defined as the the ratio of viscosity to thermal diffusivity
  $Pr = \frac{\nu}{\alpha}$

- Weber number, defined as the ratio of inertia to surface tension forces $We = \frac{\rho U^2 2R_s}{\sigma}$

- Reynolds number, defined as the ratio of inertia to viscous forces $Re = \frac{UR_s}{\nu}$

- Lewis number, defined as the ratio of thermal to mass diffusivity $Le = \frac{\alpha}{D}$

Vaporization will take place when the Peclet is very small. In this case, the droplet composition and its temperature distribution is spherically symmetric. The droplet Reynolds number is very small, almost zero, the Lewis number is not unity, but it is known for both water and acetone.

Starting with the general (differential) form of the mass, species i and energy conservation equations (with no reaction) in the gas phase, hence for $r > R_s$:

$$\frac{\partial \rho}{\partial t} + \frac{1}{r^2}\frac{\partial}{\partial r}(\rho r^2 v) = 0 \tag{3.1}$$

$$\rho\frac{\partial Y_i}{\partial t} + \rho v\frac{\partial Y_i}{\partial r} - \frac{1}{r^2}\frac{\partial}{\partial r}(\rho r^2 D_i \frac{\partial Y_i}{\partial r}) = 0 \tag{3.2}$$

$$\rho C_p\frac{\partial T}{\partial t} + \rho v C_p\frac{\partial T}{\partial r} - \frac{1}{r^2}\frac{\partial}{\partial r}(k r^2 \frac{\partial T}{\partial r}) = 0 \tag{3.3}$$

Dimensional analysis is used on this particular problem to simplify the equations. Liñán[46] showed that the heat conduction time within the drop is much smaller than the droplet life time, and the response time of the gas phase is much smaller than both the heat-up time and the heat conduction time. These simplifications together with the fact that the average droplet density (liquid) is much greater than the average gas phase density, a uniform and quasi-steady approximation can be used ($\frac{\partial}{\partial t} = 0$).

The simplified equations, however, cannot be solved without boundary conditions. These three equations can be particularized at the droplet surface, and thermodynamic equilibrium will be enforced at the surface through the Clausius - Clapeyron relation, which states the mass fraction of species i vaporized as a function of the thermodynamic properties of the components.

A dimensionless vaporization rate is defined:

$$\lambda = \frac{\dot{m} C_p}{k R_s} \tag{3.4}$$

The system can then be further simplified taking the following form:

$$\lambda = \ln(1 + C_p \frac{[T_\infty - T_s]}{L'}), \qquad \text{where} \quad L' = L_v + \frac{R_s^3 \rho_l C_l}{3\dot{m}} \frac{dT_s}{dt} \tag{3.5}$$

$$Y_s = \frac{M_v}{M} e^{(\frac{M_v L_v}{R T_B} - \frac{M_v L_v}{R T_s})}, \qquad \text{where} \quad \frac{M_v}{M} = Y_s + \frac{M_v}{M_a}(1 - Y_s) \tag{3.6}$$

$$\frac{dR_s^2}{dt} = -\frac{2k\lambda}{\rho_l C_p} \tag{3.7}$$

When λ is assumed to be constant, under the before mentioned simplifications (still unknown though), equation 3.7 reveals that the square of the droplet radius decreases linearly with time. Equation 3.8 is usually called the "d-square Law".

$$R_s^2 = -\frac{2k\lambda}{\rho_l C_p} t + R_0^2 \tag{3.8}$$

With equations 3.5 and 3.6, the dimensionless vaporization rate, the vapor mass fraction and the droplet surface temperature can be calculated.

3.2 Model I: Vaporization of a Colloidal Suspension Droplet

As the drop begins to travel in the hot environment, we will assume that the time needed for the heat from the ambient to heat the full droplet is very small compared to the vaporization time (later to be checked). Therefore, we assume that the steady-state droplet temperature is instantly reached. The transient stage of heating of multicomponent spray droplets was studied by Frolov et al [47], while Antaki and Williams [48] studied the transient processes on non-rigid slurry droplets, which are more similar to a suspension drops.

A droplet of colloidal suspension with the carrier fluid being a Newtonian fluid, will vaporize the liquid the same way as a pure, monocomponent liquid droplet, is
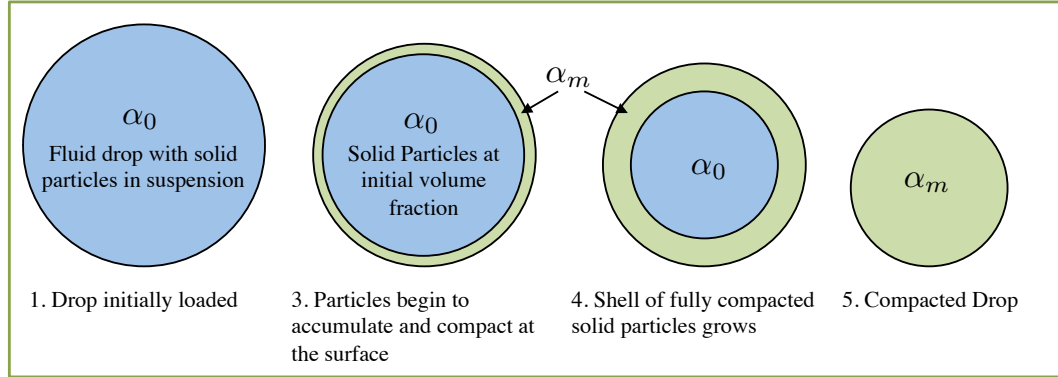
Figure 3.1: Stages of the vaporization that a colloidal suspension drop will undergo

vaporized. At the droplet surface, there are zones where the interface is liquid/air and others where it is solid particle/air. Because the temperature and concentration gradients between the liquid/air and solid/air interfaces are very small compared to external concentration gradients due to a short characteristic time of equalization, the pressure at the droplet surface (at any point) can be considered as the solvent vapor pressure, and the vaporization can be then calculated as on a pure liquid droplet.

As the liquid begins to vaporize form the surface, the solid particles will begin to move inwardly and radially getting closer together (see figure 3.1). Instantly the very first layer of solid particles will be compacted at its maximum packing number. The wet shell has been formed. The surface tension acting upon the solid particles will bring them together, accumulating them at the layer immediately after the surface layer, while the liquid moves out radially outwards to maintain the vaporization at the surface. As vaporization continues, the shell will increase in thickness, as the inner core radius R_i decreases more rapidly than liquid vaporizes at the surface.

3.2.1   Diffusion Considerations

A colloidal suspension has a continuous liquid phase in which small particles of solid are suspended. Since the solid particles suspended have a small size compared to the droplet size, Brownian motion and its effect upon the solid particles diffusing them within the liquid, may have to be considered when solving this problem. Brownian motion is characterized by its Brownian diffusion coefficient $D_{BR} = k_B T b$, where

b is the "mobility", which, for a spherical particle, is $b = \frac{1}{6\pi\mu R_{part}}$ and the diffusion characteristic time, which in this case is the time needed for the solid particles to travel a characteristic length of the order of the droplet radius $t_{BD} = R_0{}^2/D_{BR}$. This time then needs to be compared to the droplet vaporization time, which is $t_{vap} \sim \frac{\rho_l C_{pg} R_0{}^2}{2\lambda k_g}$ [49, 50].

Two limiting cases may be of relevance in suspension drops vaporization:

1. **Frozen limit fluid**. When $t_{BD} >> t_{vap}$, the time needed for a particle to diffuse a length of R_0 is much larger than the vaporzation time. Therefore, brownian motion is negligible during the droplet life time, and the solid particles can be considered to be suspended, frozen and moving only due to compactation and surface regression.

2. **Well mixed homogenous fluid**. When $t_{BD} << t_{vap}$, the time needed for a particle to diffuse a length of R_0 is much smaller than the vaporization time. Therefore, brownian motion of the particles is so rapid that in a very short time the suspension is well mixed and the droplet can be considered to be composed of a homogenous fluid with average density $\bar{\rho}$.

Comparing the two characteristic times involved in this problem, both in water and acetone-based cases:

$$\frac{t_{BD}}{t_{vap}} >> 1$$

Therefore, when studying suspension droplets vaporization, the drop can be assumed to be in the **frozen limit**.

3.2.2 Conservation Equations

The suspension within the core remains unchanged, with the same initial volume fraction of solid particles and the liquid at rest. This shell thickenning ends when $R_i = 0$ and all the droplet is fully packed at the maximum solid packing. At this time, t_f, the liquid inside the droplet has not yet fully vaporized, and the radius of the droplet is R_f.

Since the number of solid particles of the droplet do not change, there are two additional conservation equations: the volume of solid particles, as well as the liquid mass conservation equation. If the initial volume fraction of solid particles is α_0 and the maximum packing of the solid particles is α_m:

Solid Volume Conservation

The initial volume occupied by the suspended particles must equal the volume occupied by them at all times. since the particles are distributed partially in the shell (at volume fraction α_m) and in the inner core (at volume fraction α_0), the conservation equation is stated as follows:

$$\frac{d}{dt}(\frac{4}{3}\pi R_0{}^3 \alpha_0) = \frac{d}{dt}(\frac{4}{3}\pi (R_s{}^3 - R_i{}^3)\alpha_m) + \frac{d}{dt}(\frac{4}{3}\pi R_i{}^3 \alpha_0) \qquad (3.9)$$

Liquid mass conservation

The amount of liquid at all times within the droplet is distributed at the inner core (at volume fraction $1 - \alpha_0$) and at the outer shell (at volume fraction $1 - \alpha_m$). This mass of liquid must be the subtraction to the mass of liquid at the beginning of vaporization of the amount of mass vaporized at the droplet surface, per unit area (m_l'').

$$\rho_l \frac{4}{3}\pi (R_s{}^3 - R_i{}^3)(1 - \alpha_m) + \rho_l \frac{4}{3}\pi R_i{}^3 (1 - \alpha_0) = \rho_l \frac{4}{3}\pi R_0{}^3 - 4\pi R_s{}^2 m_l'' \qquad (3.10)$$

From the energy and Clausius-Clapeyron equations 3.5 and 3.6 , the amount of liquid mass vaporized per unit area can be re-written in terms of λ, T_∞, R_s, and T_s, as follows:

$$4\pi R_s{}^2 m_l'' = 4\pi R_s{}^2 k_g \frac{T_\infty - T_s}{R_s} \frac{\lambda}{e^\lambda - 1} \qquad (3.11)$$

Combining both solid and liquid conservation equations, we get the same **"d-square Law"** than in the pure liquid droplet case:

$$R_s^2 = -2\lambda \frac{k_g}{\rho_l C_{pg}} t + R_0^2 \qquad (3.12)$$

We can then conclude that the final set of equations to solve is 3.6, 3.4, 3.11, and 3.8.

3.2.3 Shell Thickenning Stage

Since the solid particles cannot leave the droplet, the regression of the surface drags the particles radially inwards and ejects the solvent outwards for vaporization at the surface, due to a pressure graient within the dorplet. As the surface regresses, the particles are packed at the surface at their maximum volume fraction, time at which the shell is formed. The more solvent vaporizes, the thicker this shell of maximum packing of particles becomes, until the whole droplet is fully packed with particles and no more solvent can be vaporized at the surface.

Case of fluid Carrier with $T_B > T_\infty$

The ratio $L_v M_v / R T_B$ that appears in the Clausius-Clapeyron equation typically ranges from 10 to 15. We can then study the vaporization process on the asymptotic case $L_v M_v / R T_B >> 1$. If the carrier fluid used in the suspension is such that $T_B > T_\infty \sim T_s$, from equation 3.6 one can conclude that the mass fraction of liquid vaporized at the surface is small $Y_{lv,s} << 1$, hence some further simplifications can be made in the previous system of equations:

$$\lambda = \frac{1}{Le} Y_s \qquad \lambda << 1 \tag{3.13}$$

$$Y_s = \frac{M_{lv}}{M_a} e^{\left(\frac{M_v L_v}{R T_B} - \frac{M_v L_v}{R T_s}\right)} \tag{3.14}$$

Since $\lambda << 1$, equation 3.11 can be re-written as:

$$C_{pg}(T_\infty - T_s) = \beta \lambda \frac{R T_B}{M_v} \tag{3.15}$$

And finally, since $\lambda = const.$ we can integrate equation 3.12

$$R_s{}^2 = -\frac{2\lambda k_g}{\rho_l C_{pg}} t + R_0^2 \tag{3.16}$$

We can then find how the inner radius decreases in time, since:

$$R_i{}^3 = R_s{}^3 \frac{\alpha_m}{\alpha_m - \alpha_0} - R_0{}^3 \frac{\alpha_0}{\alpha_m - \alpha_0} \tag{3.17}$$

The droplet will be fully packed when $R_i = 0$, hence,

$$R_f = R_0 (\frac{\alpha_0}{\alpha_m})^{1/3} \quad \text{at time} \quad t_f = \frac{\rho_l R_0{}^2}{\rho_g 2\lambda\alpha_g}[1 - (\frac{\alpha_0}{\alpha_m})^{2/3}] \tag{3.18}$$

where α_g is the diffusivity of the gas through which the liquid vapor is diffusing.

Substituting 3.13 , 3.16 and 3.14 in3.15, we obtain a trascendental equation for T_s that needs to be numerically solved.

$$\frac{1}{Le} \exp(\frac{M_v L_v}{RT_B} - \frac{M_v L_v}{RT_s}) = \frac{C_{pg} M_a}{L_v M_v}(T_\infty - T_s) \tag{3.19}$$

Case of fluid carrier with $T_B \sim T_\infty$

If $L_v M_v / RT_B >> 1$ but the ambient temperature is high and close to the liquid boiling temperature, the vaporization rate will be close to unity, and the mass fraction of liquid vaporized will not be small enough, therefore not being able to simplify as in the previous case. The equations to solve are:

$$Y_s[1 - (1 - \frac{M_v}{M_a}) \exp(\frac{M_v L_v}{RT_B} - \frac{M_{lv} L_v}{RT_s})] = \frac{M_v}{M_a} \exp(\frac{M_v L_v}{RT_B} - \frac{M_v L_v}{RT_s}) \tag{3.20}$$

$$\lambda = \frac{1}{Le} \ln \frac{1}{1 - Y_s} \tag{3.21}$$

$$C_p(T_\infty - T_s) = L_v(e^\lambda - 1) \tag{3.22}$$

However, these conditions will never be met during the coating process in the pharmaceutical industry, since these high ambient temperatures would cause the rapid packing of the droplet before coating the tablet, and the beginning of the formation of a bubble, an undesired process. Nevertheless for process completeness, the bubble formation stage is described in the next section.

3.2.4   Vapor Bubble Formation Stage

For times $t > t_f$, and only if the ambient temperature is high enough, a vapor bubble is created inside the compacted droplet ([19]), wth a radius R_b, with the voids between the solid particles filled with the vapor of the liquid at the vapor pressure $p_v = p_a \exp(\frac{M_v L_v}{RT_B} - \frac{M_v L_v}{RT_s})$, with a negligible density compared to the liquid density $(\rho_{lv,bubble} << \rho_l)$.

The liquid that vaporizes at the external surface (with a constant radius R_f) comes from the liquid originally in the compacted bubble region of radius R_b and displaced by the formation of the bubble, so that:

$$\dot{m}_l = \frac{d}{dt}[\frac{4}{3}\pi R_b{}^3(1 - \alpha_m)\rho_l] = \frac{1}{L_v}4\pi R_f{}^2 k_g \frac{T_\infty - T_s}{R_p}\frac{\lambda}{e^\lambda - 1} \tag{3.23}$$

This expression will allow us to find the temporal evolution of the size of the vapor bubble $R_b(t)$. As liquid is being pushed away from the inner core towards the surface from the bubble, it will move through the compacted porous media if there is enough pressure gradient between the inner interface and the liquid/gas interface.

At the inner interface, for $r < R_b$, the bubble will be at the vapor pressure, while for $r > R_b$ there will be water. However, since there are also solid particles at the interface, the liquid will try to wet the interior surface of these particles, meaning that $p_v - p_l > 0$. Moreover, this pressure difference is due to surface tension of the liquid between two solid particles $p_v - p_l \sim \sigma/d_p$, where d_p is the particles diameter. This pressure gradient will alllow the bubble to grow and push the liquid radially outwards.

In [20] different cases of drop vaporization and bubble formation are investigated, suggesting the different morphologies that the drop can undergo depending on ambient conditions.

However, as previously noted, this vapor bubble will form only and if only the temperature of the surrounding air and hence the temperature of the drop, as well as the pressure within the drop are high enough so as to form this vapor bubble inside the drop. These conditions will not be reached in the coating process under no circumstances, since the temperature of the drying air will have a maximum value of approximately $T_\infty = 60\,{}^oC$.

3.3 Model II: Vaporization of a Multicomponent Solution Droplet

The drop fluid is a very diluted solution, composed of a solvent, typically acetone, different polymeric solutes and a passive fluid, typically water. As the vaporization progresses, since the amount of solute is given by the initial solute loading, the mass fraction of solute increases, relatively speaking, as solvent is leaving the drop. The drop will keep increasing its solute concentration until it reaches a critical concentration, the saturation mass fraction.
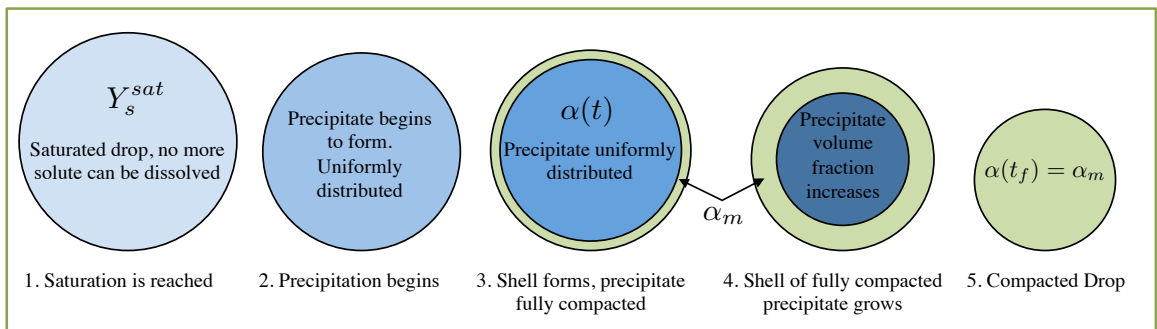
Figure 3.2: Stages that a solution droplet will undergo during vaporization. Size and composition will change temporally and spatially

When a solution reaches its saturation point at time $t = t_{sat}$, if more solute is added, or like in this case, more solvent is removed, the extra solute will precipitate and solidify in various forms depending on the solute composition. Polymeric solutes precipitate in form of entangled fibers. However, in order to model both the precipitation and the vaporization process, a precipitated volume fraction defined as the ratio of the equivalent volume of "n" spherical particles (of radius r_{part}) with the precipitated solute density to the volume of precipitated solid. Thus, the precipitated volume fraction is defined in terms of the amount of precipitated solute occupying a sphere of generic radius R, as:

$$\alpha = \frac{n \frac{4}{3}\pi r_{part}^3 \rho_s}{\frac{4}{3}\pi R^3 \rho_s} \tag{3.24}$$

Figure 3.2 shows a sketch of the suggested process. Immediately after pre-

cipitation begins to occur, the precipitate will distribute uniformly throughout the droplet volume. Because the solvent will continue to vaporize, more solute will precipitate (drop is saturated at all times). But also, as the drop is vaporizing solvent, the relative concentration of solute increases, and since saturation conditions need to be kept, more solute will precipitate in the drop.

As the drop volume decreases, the precipitate (particles in our model) will begin to gather at the surface and compact as a fully packed surface layer of precipitate. The more solvent is vaporized at the surface, the thicker this compacted layer (outer shell) will grow, and the smaller the inner core will be. The process will continue until the entire drop is fully compacted at the maximum packing α_m.

3.3.1 Drop Shrinkage

A solution drop of initial radius R_0 of a specific composition (total solutes mass fraction X_0) is initially sprayed at a certain air jet speed V_0 in a dry ambient with temperature T_∞.

As a result of the vaporization occurring at the surface, the drop will begin to shrink. Like in the suspension case, vaporization occurs and continues because of the diffusion of the solvent vapor through the gas phase; far away from the drop the mass fraction of solvent vapor is zero, a gradient of vapor concentration will then develop enabling diffusion to carry the solvent vapor away from the surface, enabling the vaporization to continue at the surface.

Since the drop is being carried by the air, the relative speed of the drop to the air is negligible. The equations of a pure liquid droplet vaporization will hold, since the solution is very diluted and the only species vaporizing is the solvent. Like in the simple case, once λ is known, the radius squared $R_s(t)^2$ will decrease with time as:

$$R_s(t)^2 = -\frac{2\lambda k_g}{\rho_{solv} C_{pg}} t + R_0^2 \tag{3.25}$$

To find λ , the equation to solve is 3.15, as in the pure liquid and suspension cases.

The amount of solvent vaporized can be found recalling the definition of λ from equation 3.4. Integrating $\dot{m}(t)$, we obtain:

$$m_{solv,v} = \int_0^t \dot{m} \, dt = -\frac{1}{3}\rho_{solv}R_s^3(t) \tag{3.26}$$

At any given time $t < t_{sat}$, the total mass of the drop can be calculated as:

$$m_t = m_{solu}(t) + m_{t,0} - m_{solv,v}(t) \tag{3.27}$$

Therefore,the mass fraction of solute can be computed:

$$Y_s(t) = 1 - \frac{m_{t,0}}{m_t(t)} + \frac{m_{solv,v}(t)}{m_t(t)} \tag{3.28}$$

3.3.2   Saturation Conditions

When the drop reaches saturation conditions, the solute mass fraction will equal the critical value $Y_{solu,sat}$. Knowing that the solute does not leave the droplet:

$$m_{s,0} = m_{s,sat} = Y_{solu,sat}m_{t,sat} \tag{3.29}$$

and that the drop is assumed to be spherical:

$$m_{t,sat} = \frac{4}{3}\pi R_{s,sat}^3 \rho_{mix} \tag{3.30}$$

We can find the drop radius at this sauration point, and the time at which it happens:

$$R_{s,sat} = R_0 \left(\frac{\rho_{s,p}X_0}{Y_{solu,sat}\rho_{mix}}\right)^{1/2} \tag{3.31}$$

$$t_{sat} = (R_0^2 - R_{s,sat}^2)\frac{\rho_{solv}C_{pg}}{2\lambda k_g} \tag{3.32}$$

3.3.3   Shell Formation and Thickenning

Once the drop reaches saturated conditions, and continues undergoing vaporization for $t > t_{sat}$, there will be an excess of solute (it cannot leave the drop) which will begin to precipitate. Now the drop will have three different components: solvent and solute in saturation, and precipitated solid.
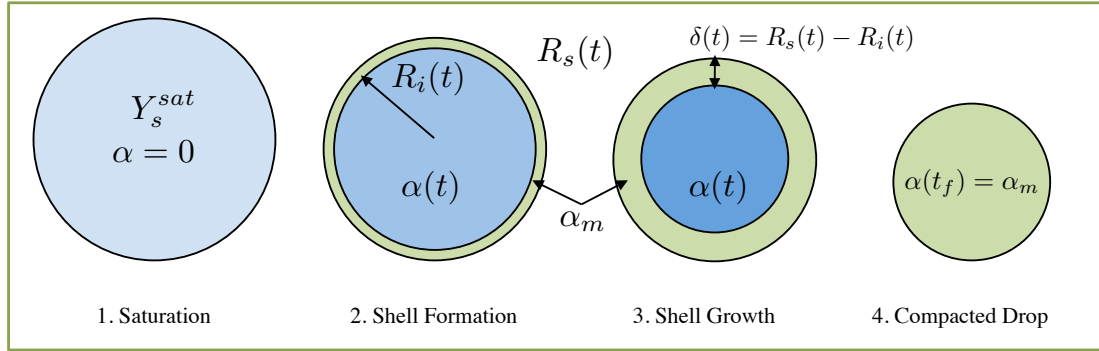
Figure 3.3: Mathematical model and variables during drop vaporization

$$m_t(t) = m_{solu,sat}(t) + m_{solv} + m_{solu,p}(t) \tag{3.33}$$

As soon as some precipitate is formed, it will be uniformly distributed within the drop with a volume fraction $\alpha(t)$. However, since the drop will continue to shrink and more precipitate will form, although at the beginning uniformly distributed, $\alpha(t)$ will increase, and within a very short period of time a very thin layer of precipitate will accumulate at the surface of the drop (see figure 3.3). This layer will be composed of solid particles packed at their maximum packing (α_m), and saturated solution in the voids in between particles.

As solvent vaporizes at the drop surface (R_s), more precipitate will form and the shell at volume fraction α_m will continue growing in thickness $\delta(t) = R_s(t) - R_i(t)$; while the inner core of the drop will decrease in size. This inner core will be composed of saturated solution and uniformly distributed precipitate with increasing volume fraction $\alpha(t)$.

The mass of precipitated solute will be distributed between the inner core and the outer shell:

$$m_{solu,p} = \frac{4}{3}\pi(R_s^3(t) - R_i^3(t))\rho_s\alpha_m + \frac{4}{3}\pi R_i^3(t)\rho_s\alpha(t) \tag{3.34}$$

The amount of solute that is precipitated at any given time $t > t_{sat}$ is due to solvent vaporizing at the surface:

$$m_{solu,p} = (m_{t,sat} - m_{solv,v}|_{t_{sat}}^{t})(1 - Y_{solu,sat}) - (m_{solv,sat} - m_{solv,v}|_{t_{sat}}^{t}) \qquad (3.35)$$

Hence, using equations 3.26 ,3.35 and 3.34 we obtain a single equation which contains the two unknowns, $R_i(t)$ and $\alpha(t)$.

$$
\begin{aligned}
R_i^3(t)(\alpha(t) - \alpha_m) = -R_s^3(t)\left[\alpha_m + Y_s^{sat}\frac{\rho_{solv}}{4\pi\rho_s}\right] + Y_{solu,sat}\frac{\rho_{solv}}{4\pi\rho_s}R_{s,sat}^3+ \\
+\frac{3}{4\pi\rho_s}[m_{t,sat}(1 - Y_s^{sat}) - m_{solv,sat}]
\end{aligned}
\qquad (3.36)
$$

Chapter 4

Results

4.1 Application of the Quasi Steady-State Vaporization Models to the Particular Problem of Tablets Coating

The models outlined in previous chapters, for both types of fluids drops have been developed on an idealized or theoretical environment. However, the actual environment and conditions at which tablets coating is performed are far more complex than the idealized problem. In the previous chapter, we have studied the case of the quasi-steady state evaporation of suspension and solution droplets in a moderately hot environment, with spherical symmetry, negligible Brownian diffusion within the drop, and negligible relative speed to the air of the droplet.

During the coating process, a bed of tablets sits on a rotating drum; the drum is provided with an atomizer, through which the drops of the coating solution are sprayed, as the drum rotates. Simultaneously, two orifices provide the drum with the drying air, two air jets at low speed but high temperature, ranging from $25 - 60\,^oC$.

Therefore, the actual problem of tablets coating can be represented as in figure 4.1. Under an environment with ambient temperature $T_{drying\,air} = T_\infty$, the atomizer, located at a distance L from the tablet, sprays droplets of a particular composition, with an initial diameter (at $4 - 6$ in from atomizer) D_0, initial speed V_0. While traveling the distance L, the droplet undergoes a vaporization process as well as a change

in composition and morphology. Depending on the parameters aforementioned, when the droplet finally impacts the tablet, it may or may not have formed a shell, and if it has formed, the thickness of this wet shell will vary depending on these parameters.

One main assumption made in the following calculations is that the droplets will not interact with each other. Since they are several drop diameters away one to another and since a constant low speed stream of air (drying air) is provided into the rotating drum (providing a continuously dry environment) the vaporization of one droplet will not affect the vaporization of another one, since the solvent vapors will be carried away by the surrounding air stream.
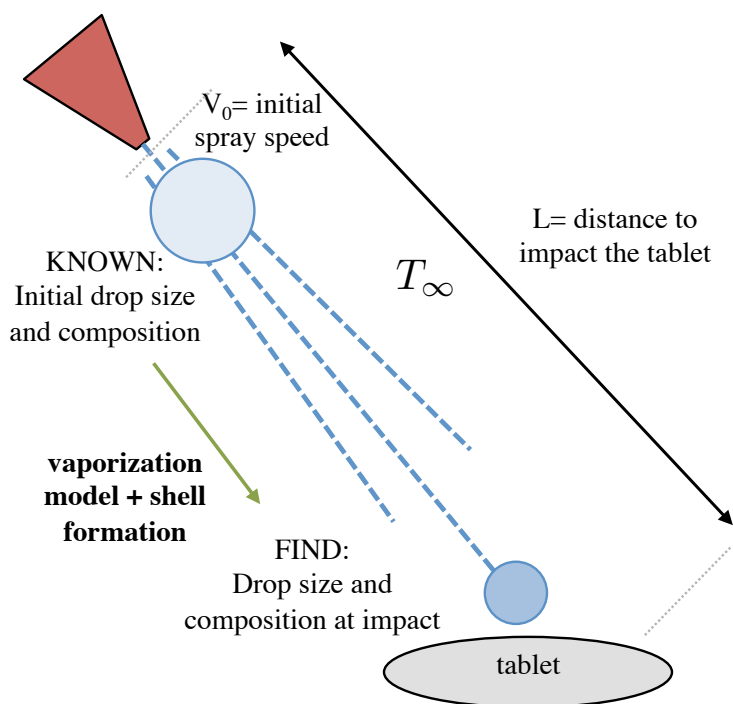
Figure 4.1: The particular problem of tablets coating. From atomization to impact.

A MatLab program to simulate this process was developed. As it can be seen in figure 4.2, the input parameters are the temperature of the drying air, atomization gas velocity (a characteristic initial speed of the drop), the distance from the atomizer to the bed of tablets, the initial drop SMD (Sauter Mean Diameter) and the droplet composition. When the button *Compute* is hit, two plots will be produced: one (on the bottom left of the window) showing the evolution in time of the surface (yellow)

and inner (magenta, if the shell was formed) drop radii, and a secondary plot (top right of the window) of the shell thickness as a function of time. In the lower right corner the different times involved in the process are displayed, such as time to impact the tablet, time to reach saturation in the drop and the time at which the program finalizes the calculation.The program also displays a text reporting whether a shell was formed or not depending on the initial conditions, and a text file is created, where the initial parameters as well as the size and composition time evolution are stored.

Using this program, we are able to perform a parameters study to observe the effect of the different input parameters on the shell formation and its thickness, during the coating process.

4.2   Deceleration and Impact Droplets

The time needed for the droplet to acquire its terminal speed relative to the jet of air, when drag and inertia forces are balanced, is much smaller than any of the times involved in the vaporization process or an estimate of the time to impact. Hence, we can assume that the terminal speed is instantly reached. Because the relative terminal speed of the drops to the air is very small compared to the speed of the atomization air, these drops can be considered to be flying at the air speed. The speed of the air a few inches downstream of the atomizer nozzle (when the spray is fully developed and the drops will not break any further) can vary between $20 - 80\,m/s$. The atomization and following spray becomes then a turbulent jet of two components: air and solution droplets. A turbulent jet will decrease its average velocity [52], in particular at the centerline, as a function of the distance travelled from the nozzle exit. Therefore, the droplet carried by the air, will decelerate as it travels until impacting the tablet.

In the case of single fluid round (axisymmetric) and planar (2D) jets, simplifications can be made in the Reynolds Averaged Navier-Stokes equations [54] from boundary layer theory, in order to obtain similarity solutions for the averaged variables. Because the droplets formed with the atomizer are very small and drop-diameters away one from another, we will assume the case of a single droplet traveling at the same speed that the jet of air.

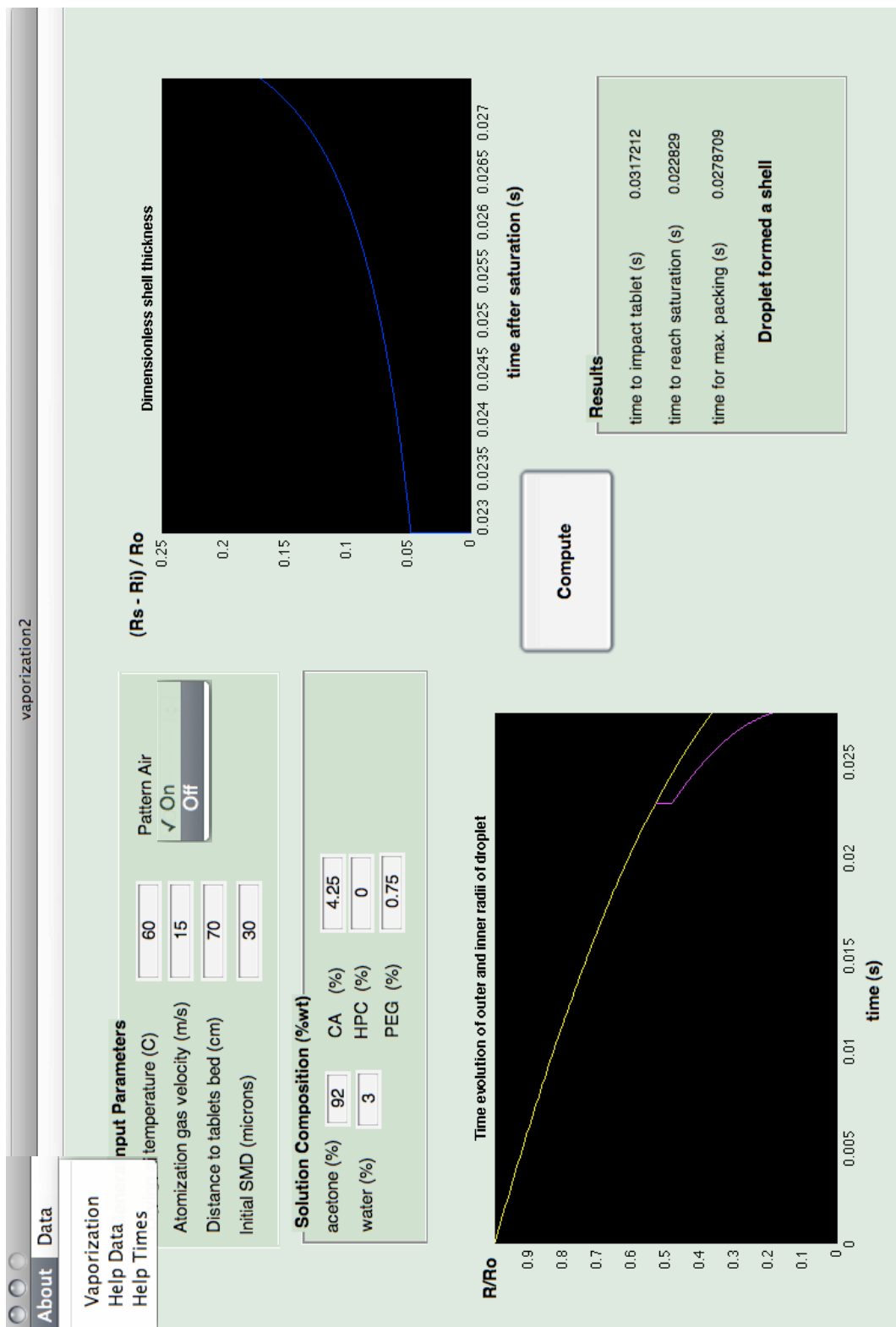The momentum transferred from the atomization air to the drop is small com-

Figure 4.2: Graphical interface of the program used to compute shell thickness and drop composition

pared to the air jet momentum. Hence, when calculating the droplet speed decrease as it travels, the drop will decrease its speed similarly to the air jet it is immersed in.

Dimensional analysis of a turbulent jet shows self-similar Gaussian-like velocity profiles that as studied sections are located further from the nozzle. Since the maximum speed in every section is located at the jet centerline, we will use the longitudinal evolution of the jet speed at the centerline in our calculation. The expressions used to compute the speed drop are taken from [55].

Both round and planar jets will be studied. If the user selects to switch the pattern air on at the program interface, the program will assume that the pattern air of the atomizer is being used, producing a slender elliptical shaped spray jet. Since the major axis of the elliptical cross section of this spray is much larger than the minor axis, a planar jet approximation can be made to compute the decrease in the drop speed. On the other hand, when the pattern air is off, the jet is more likely to have circular cross section, and the equations for a round jet will be used to obtain the evolution of the drop speed.

4.3   Vaporization of a Colloidal Suspension Droplet

Let us recall that a colloidal suspension droplet is composed of small solid particles within a carrier fluid, either acetone or water. As the drop is immersed in a hot environment, only the carrier fluid will vaporize at the droplet surface. For the droplets of colloidal suspension, the study focuses on the effect of ambient temperature, initial solid loading, maximum packing and initial droplet size.

4.3.1   Effect of Droplet Initial Radius

As the initial drop radius is increased, figure 4.3 shows a predicted increase on the time needed to reach maximum packing in the droplet. The "d-square law" predicts a slope only dependent on the vaporization rate λ, and gas and liquid thermodynamic properties. Hence, the rate at which the drop shrinks is not affected by the initial drop size.

It is remarkable the difference in order of magnitude of the time at which the
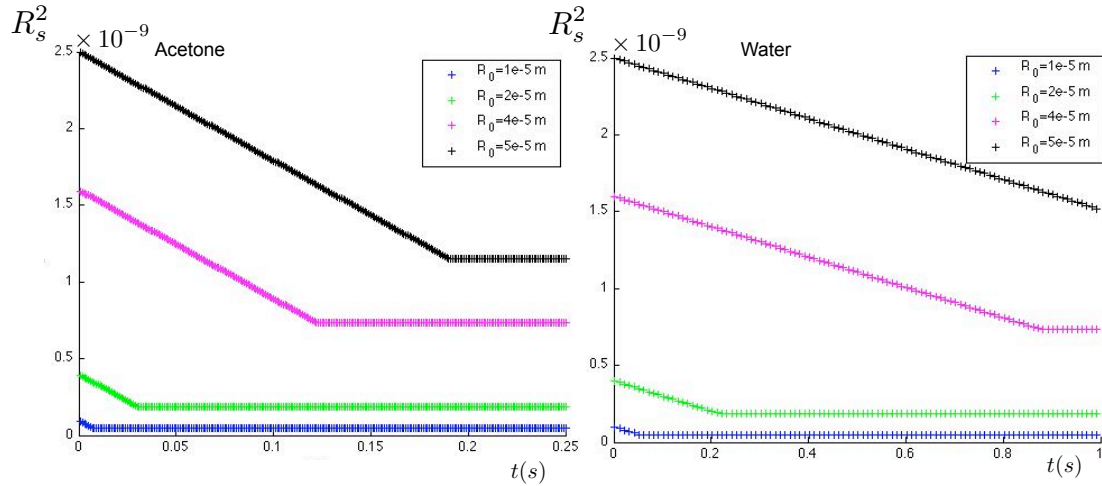
Figure 4.3: Effect of Initial Droplet Radius for Acetone and Water based solutions

maximum packing is reached depending on the carrier fluid. Acetone is a much more volatile fluid than water, its latent heat of vaporization and boiling temperature being substantially smaller than in water. This results on a larger dimensionless vaporization rate λ (for acetone-based drops $\lambda \sim 0.1$, while for water-based drops $\lambda \sim 0.01$), which simultaneously will lead to a smaller vaporization time and final time (to reach maximum packing), for the same initial drop size.

4.3.2 Effect of Ambient Temperature

Solving the set of equations for water-based and acetone-based suspension droplets for four different ambient temperatures ranging from 323 K to 353 K, we find the quasi-stationary droplet temperature, as well as the liquid vapor mass fraction leaving the droplet surface and the dimensionless vaporization rate λ. For both approaches, the final droplet radius is the same. whereas the time required to reach differ depending on the carrier fluid properties.

The initial droplet radius is $R_0 = 30\,\mu m$, the initial solid volume fraction is $\alpha_0 = 0.2$, while the maximum packing of the solid phase is taken to be $\alpha_m = 0.64$.

It is important to remark the temperatures reached by the droplet are in both cases smaller than the ambient temperature. This feature is especially dramatic for droplets with acetone as carrier fluid. Their temperatures reach values as low as 261

K. This is due to the combined effect of its low latent heat for vaporization together with the ambient temperature being higher than its surface but not sufficiently high as to heat the droplet. Therefore, the only way for the drop to exchange heat with the environment is to loose heat and cool down.

The rate at which R_s^2 decreases is higher in acetone-based than in water-based solutions, as can be observed in figures 4.5 and 4.4 the slopes of the acetone-based are steeper than the water-based at any of the four ambient temperature. In both cases the radius square decreases linearly, until reaching the maximum solid particles packing (radius R_f) when, if conditions are met, a bubble may form and grow.
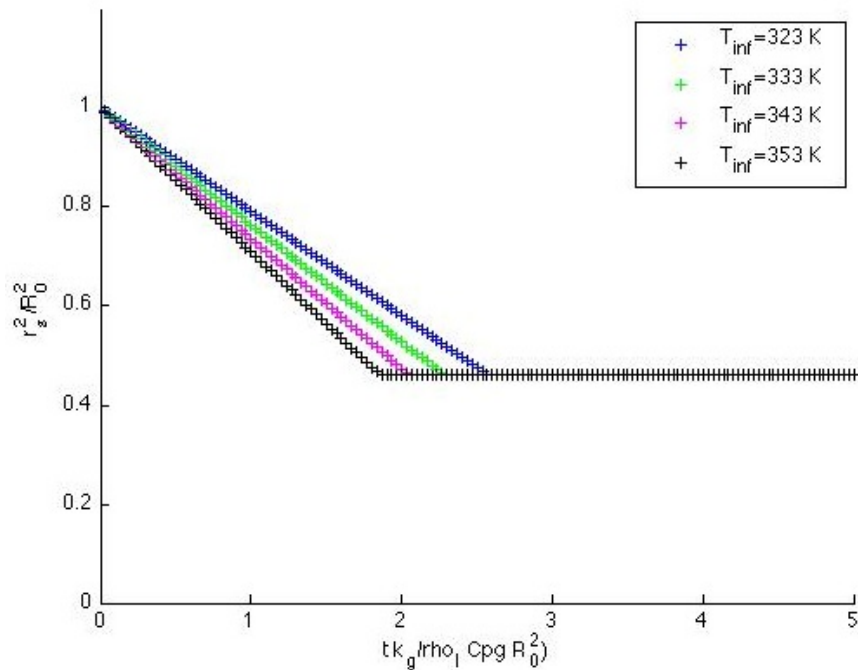
Figure 4.4: Rate of decrease of the square of the acetone droplet radius

Finally, the most important feature to note is the change of the slope in both cases with the ambient temperature. As ambient temperature is increased the slopes become steeper, meaning that the vaporization occurs faster, hence reaching earlier the fully compacted state.

One of the first simplifications when developing this model, was under the assumption of a quasi-steady state after a short transition period, when the droplet
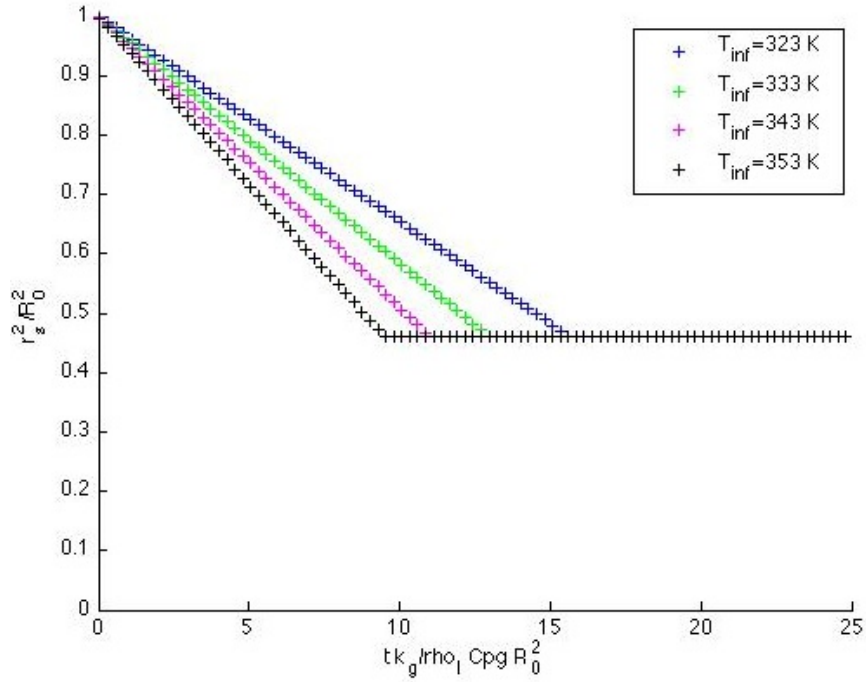
Figure 4.5: Rate of decrease of the square of the water droplet radius

is heated up reaching the steady drop temperature T_s. This assumption needs now to be checked, to make sure that this transition stage is in fact short compared to the droplet vaporization time.

The energy equation for $r < R_s$, with no internal convection and, as a first approximation, assuming that the thermodynamic properties of the droplet (mixture of solid and liquid) are similar to the properties of the liquid:

$$\rho_l c_l \frac{\partial T}{\partial t} = k_l \frac{1}{r^2} \frac{\partial}{\partial r}(r^2 \frac{\partial T}{\partial r}) \tag{4.1}$$

Taking orders of magnitude in this equation:

$$\rho_l c_l \frac{T_s - T_0}{t_{cond}} \sim k_l \frac{T_s - T_0}{R_0^2} \tag{4.2}$$

where T_0 is the initial temperature of the droplet.

Hence, the conduction characteristic time:

$$t_{cond} \sim \frac{\rho_l c_l R_0^2}{k_l} \sim \frac{R_0^2}{\alpha_l} \tag{4.3}$$

- for water: $t_{cond} \sim \frac{(3 \cdot 10^{-5})^2}{1.43 \cdot 10^{-7}} \sim 6 \cdot 10^{-3} \, s$

- for acetone: $t_{cond} \sim \frac{(3 \cdot 10^{-5})^2}{9.42 \cdot 10^{-8}} \sim 10^{-2} \, s$

Comparing these characteristic times with the vaporization time, defined as $t_{vap} \sim \frac{\rho_l C_{pg} R_0{}^2}{2\lambda k_g}$,

- for water: $t_{vap} \sim \frac{1000 \cdot 1012 \cdot (3 \cdot 10^{-5})^2}{2 \cdot 0.02 \cdot 0.024} \sim 0.95 \, s \gg t_{cond}$

- for acetone: $t_{vap} \sim \frac{790 \cdot 1012 \cdot (3 \cdot 10^{-5})^2}{2 \cdot 0.13 \cdot 0.024} \sim 0.11 \, s \gg t_{cond}$

One can then conclude that the conduction time is very small compared to t_{vap}, showing that the assumption of quasi-stationary state was correct and that droplet heat up is negligible and can be assumed that in a very short time the droplet reaches a uniform and stationary temperature T_s.

4.3.3 Effect of Initial Solid Particles Loading and Maximum Packing α_0

Recalling the stop condition at which the droplet is at its maximum solid packing:

$$R_f = R_0 \left(\frac{\alpha_0}{\alpha_m}\right)^{1/3} \quad \text{at time} \quad t_f = \frac{\rho_l R_0{}^2}{\rho_g 2\lambda \alpha_g}\left[1 - \left(\frac{\alpha_0}{\alpha_m}\right)^{2/3}\right] \tag{4.4}$$
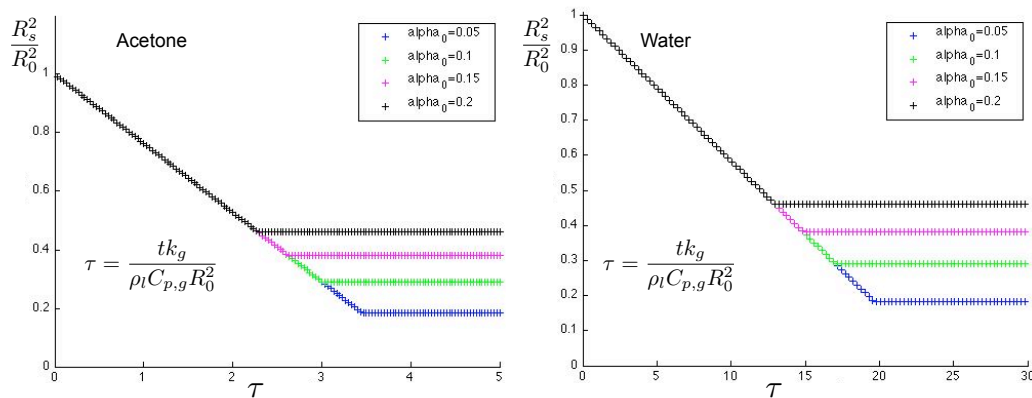
Figure 4.6: Effect of Initial Solid Particles Loading for Acetone and Water based solutions

Table 4.1: Base input parameters for the program

Parameter	Value
$Y_{s,sat}$	0.54
T_∞	310 K
L	0.7 m
V_0	15 m/s
D_0	50 microns
α_m	0.51

it is obvious to conclude that the final radius slowly increases as $\alpha_0{}^{1/3}$ while the time at which this occurs decreases as $-\alpha_0{}^{2/3}$, as can be shown in the figures below, for both water and acetone based solutions.

Figure 4.7: Effect of Maximum Solid Packing for Acetone and Water based solutions

4.4   Vaporization of a Solution Droplet

For the case of an acetone-base solution droplet, in order to be able to see the shell formation, the base input parameters were the following:

In the following sections, one parameter at a time has been varied, while the rest have been kept constant.

4.4.1 Effect of Ambient Temperature

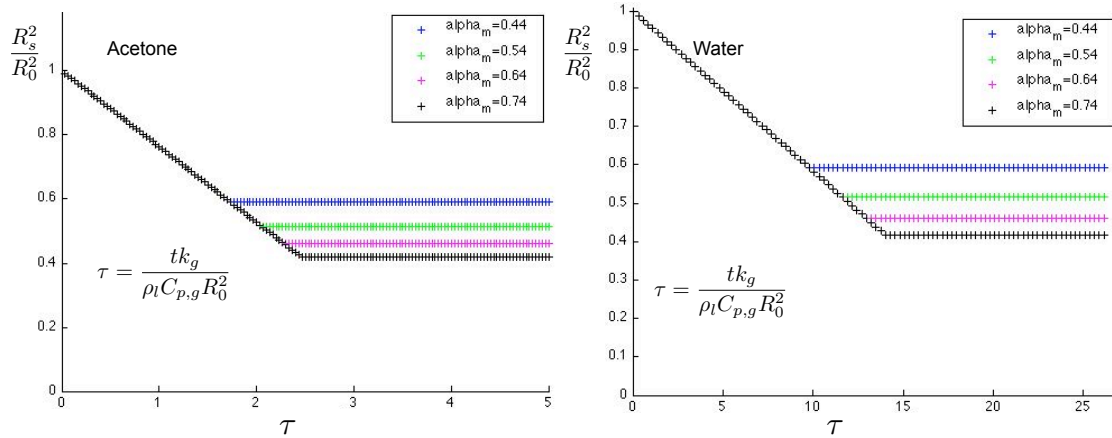As shown in the plot 4.8, as the drying air temperature increases, the shell begins to form much earlier. If the ambient temperature is increased, the saturation point will be reached earlier, hence the earlier shell formation. However, this decrease of time is not linear. The distance between curves decreases as the temperature increases. Let us recall the the ambient temperature plays its key role in the mass vaporization rate of the solvent. The higher the temperature the higher the vaporization rate λ. But also, the higher λ is, the steeper the slope of the time evolution of the radius is. These two variable then are used to calculate the inner core radius, not having then a direct relationship between temperature and shell thickness. This is what causes as well the slight difference in slope for the different drying air temperatures.
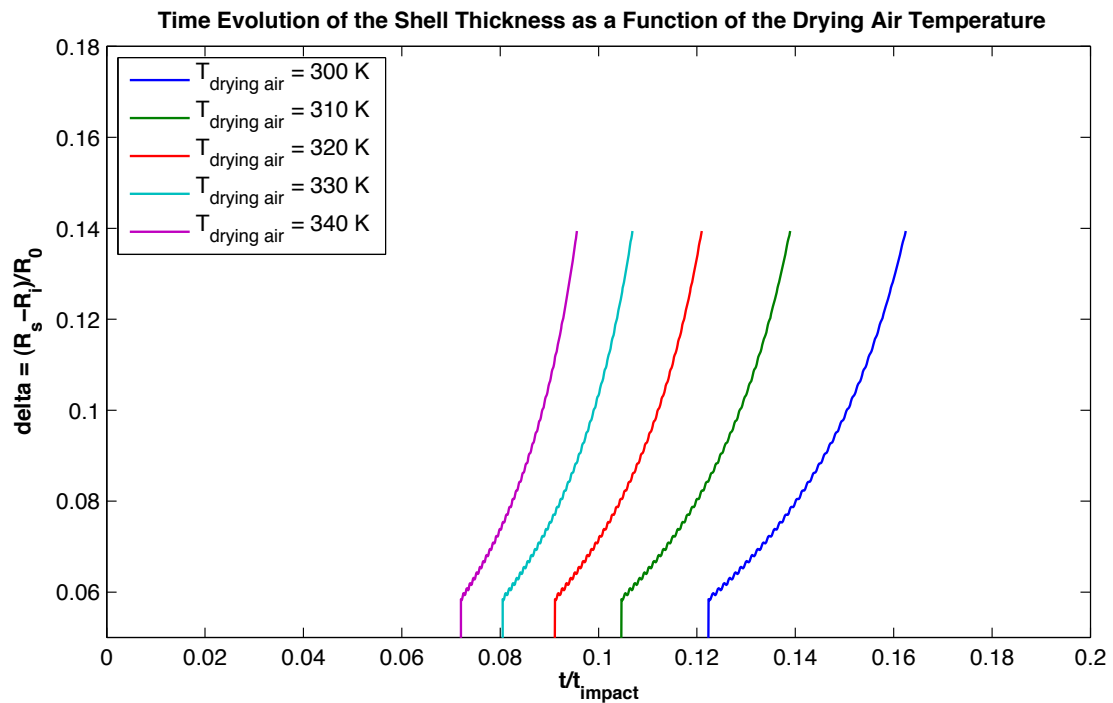

Figure 4.8: Temporal variation of the shell thickness as a function of the drying air temperature

Something to remark as well is that the shell grows very quickly right after its formation in what it seems a linear fashion, and then the growth is somewhat

relaxed, although monotonously growing. This effect is partly due to the nature of the shell growth but also partly due to the scheme to solve the equation to find the inner radius. The drop passes from not having a shell to forming and growing a shell, and since the mentioned equation has two unknowns in it (inner radius and inner core precipitate volume fraction α), we have to enforce the initial conditions at saturation point, which produces a quick growth of the shell during the first time steps of the calculation.

Time Evolution of the Inner Precipitate Volume Fraction as a Function of the Drying Air Temperature
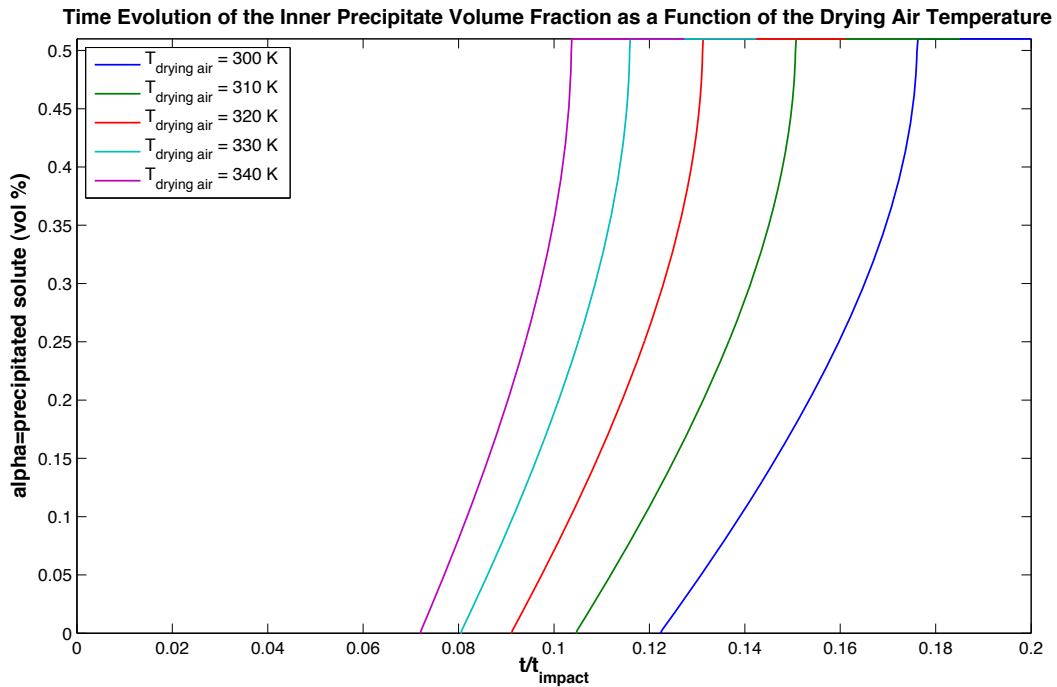
Figure 4.9: Temporal variation of the inner core precipitate solute volume fraction as a function of the drying air temperature

As explained in previous chapters, not only are we interested in drop size change, but we are also seeking the temporal variation on the droplet composition. A way to measure the droplet composition at all times is through the parameter $\alpha(t)$, the volume fraction of precipitated solute at the inner core. This parameter accounts for the amount of solute (all polymers that are in solution) that at any instant of time t is precipitated in the drop. Once the wet shell is formed, the solute can only precipitate within the inner core of the droplet. The figure 4.9 shows how the increase of the drying air temperature decreases the time at which precipitation begins to occur,

since vaporization is favored at higher temperatures. For all temperatures, when the maximum packing is reached, that is when $\alpha = \alpha_m = 0.52$, the drop cannot decrease in size, nor can it increase its precipitation. When this happens, the drop is fully packed and will not vaporize more solvent.

4.4.2 Effect of Initial Solid Loading X_0

When the initial amount of solute within the drop is linearly increased, two phenomena are observed. First, the time at which the shell begins to form decreases with increasing solute mass fraction; this is logical, since an increase of solute will induce saturation conditions much faster. Second, the slopes after the first stage of quick growth seem to be kept constant no matter what the solute mass fraction is.
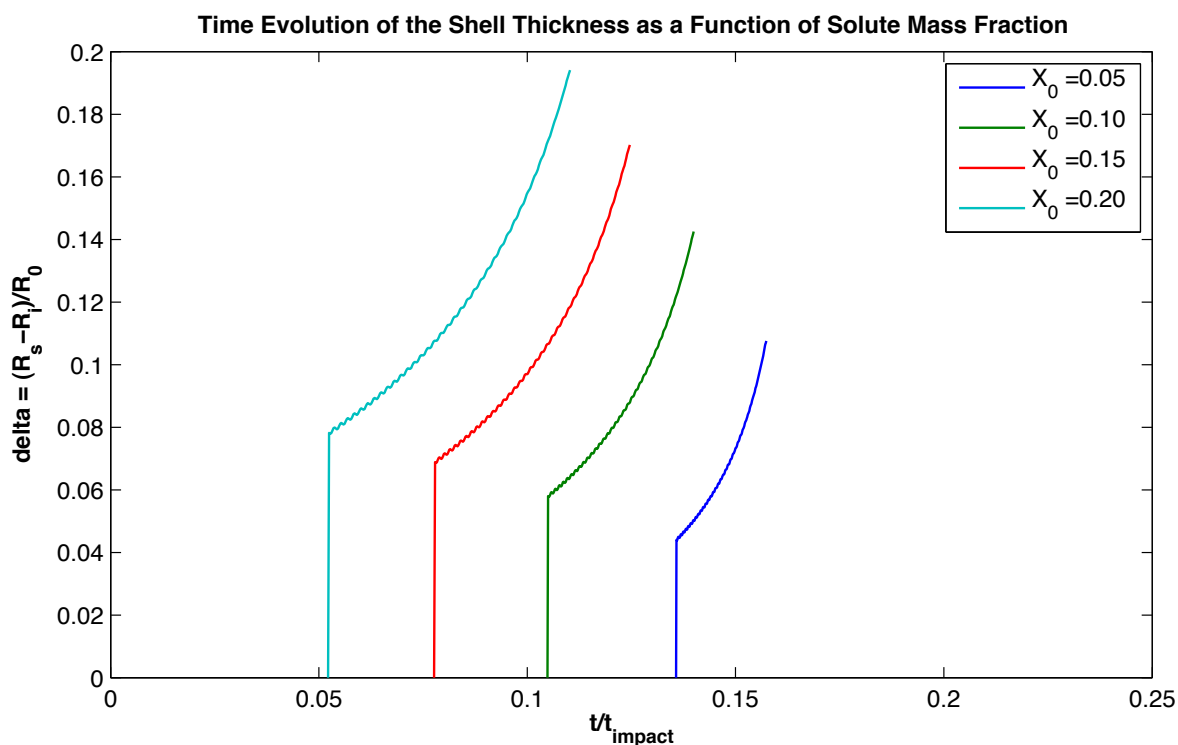

Figure 4.10: Temporal variation of the shell thickness as a function of the initial solute mass fraction

The distance between the different solute mass fraction cases seem to be

roughly the same, concluding that the relationship seems to be relatively linear. the The initial solute loading is used to calculate the initial mass of solute and through it, the amount of precipitate, which is embedded in the equation to obtain the inner radius. We can then conclude the relationship between inner core and solute mass fraction is much more direct than inner core and ambient temperature.

Time Evolution of the Inner Precipitate Volume Fraction as a Function of the Initial Solute Mass Fraction

Figure 4.11: Temporal variation of the inner core precipitate solute volume fraction as a function of the initial solute mass fraction

As for the time evolution of the composition, and increase in solute mass fraction will lead to a decrease in the time at which the shell begins to form. The parameter α begins to grow at an earlier time. However, an interesting feature to note is that, as observed in figure 4.11, the lower the solute mass fraction is, the less time the inner core precipitates take to reach their maximum packing.

4.4.3   Effect of Initial Drop Size

Larger drops will take larger times to reach the saturation conditions. The times to reach saturation seem to increase more as the drop becomes larger, be-

cause most of our equations are based in mass conservation, which involves volumes. Therefore, for instance, an increase of $10\mu m$ in radius means an increase in volume of $1000\mu m^3$, which would translate in a much larger volume, hence a much larger time to reach saturation.
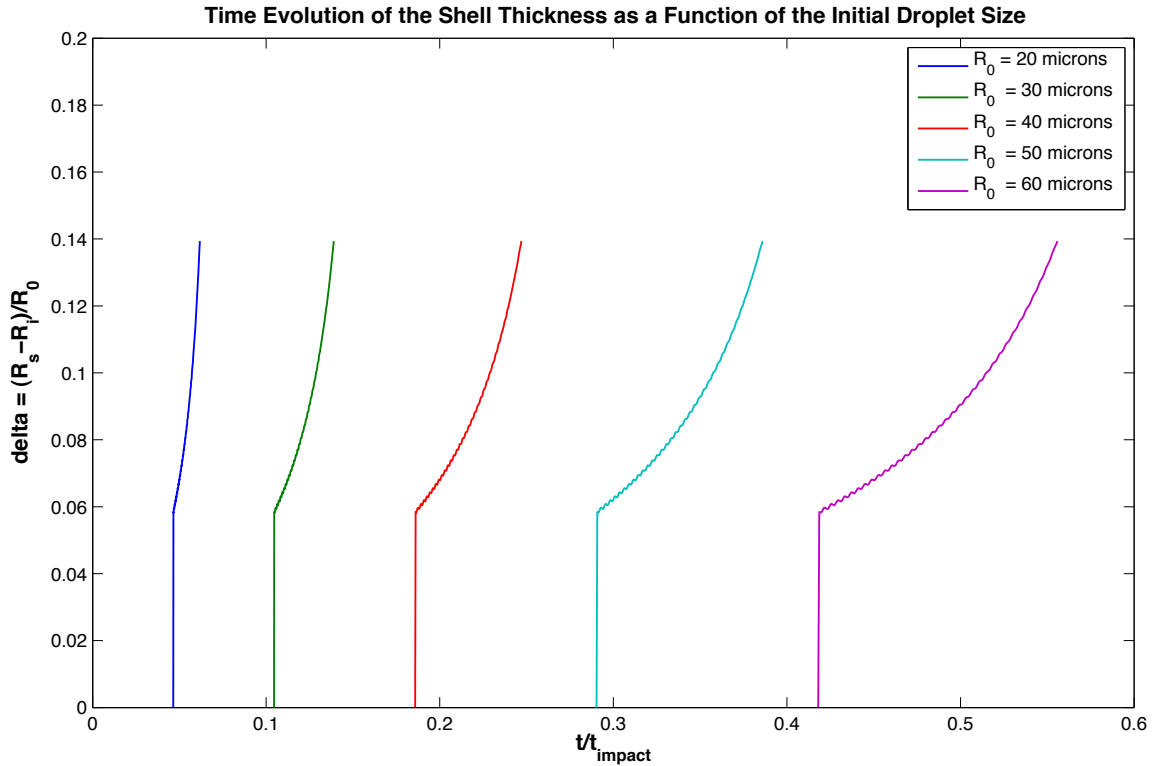
Figure 4.12: Temporal variation of the shell thickness as a function of the initial drop radius

This reasoning can also be used to explain the decrease in the slope for larger drops. The larger the radius drop is, the even larger its volume is, hence much larger time will be needed to accumulate particles at their maximum packing, to grow the shell thickness.

In figure 4.13, the time evolution of the precipitated volume fraction is plotted as a function of the initial size. Larger droplets will take larger times to begin the precipitation process, because more surface vaporization is needed in larger droplets. Again, the precipitation and thus the vaporization will stop when $\alpha = \alpha_m$. When

Time Evolution of the Inner Precipitate Volume Fraction as a Function of the Initial Radius
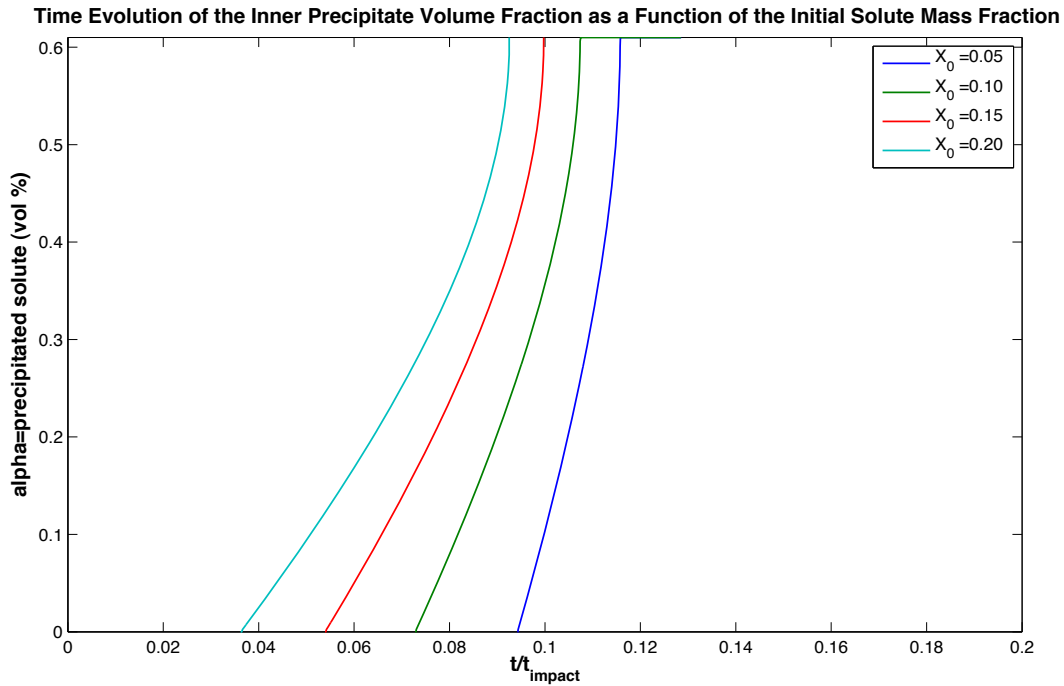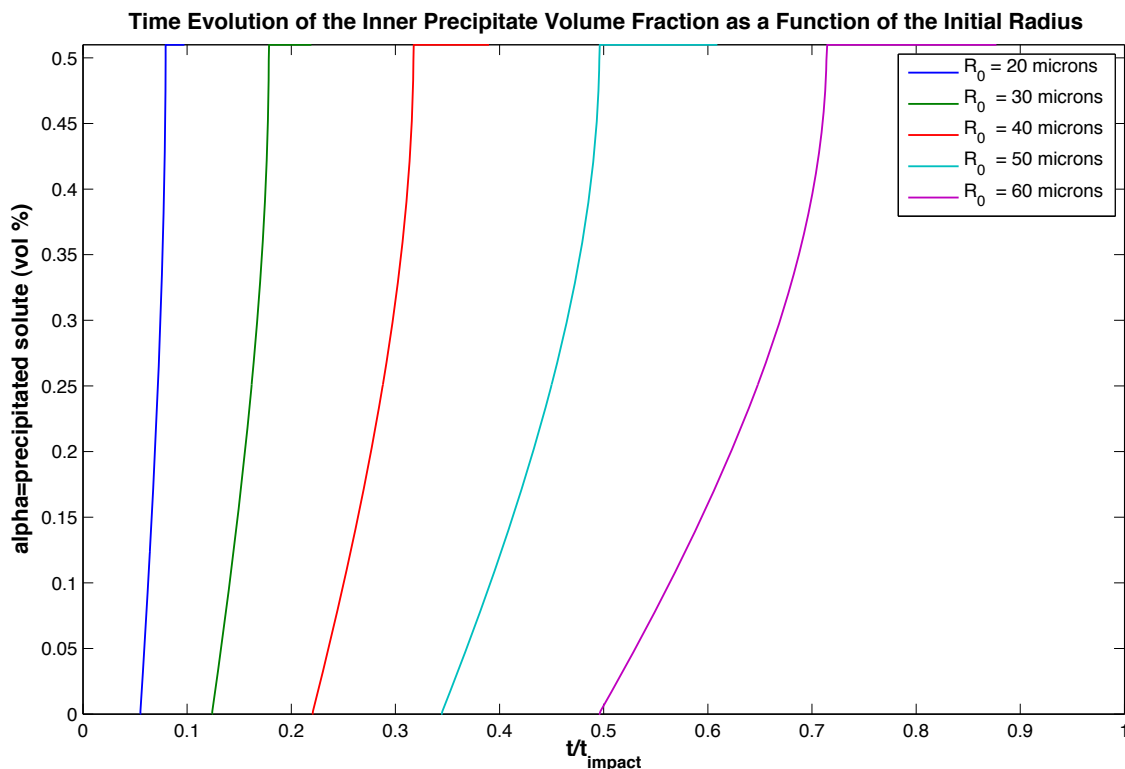

Figure 4.13: Temporal variation of the inner core precipitate solute volume fraction as a function of the initial droplet size

smaller droplets are subjected to this vaporization process less time is needed to reach the maximum packing.The parameter α is a volume-based parameter, this means that an increment in radius will translate in both a squared increment of available solvent to vaporize and a cubed increment in available volume to precipitate solute. Hence, the larger the droplet is, the more time is needed to vaporize solvent, to form the shell and to precipitate more solute after the shell formation.

4.4.4 Effect of Initial Drop Speed

The initial speed of the drop does not affect at all on the vaporization process. As observed in figure 4.14, all curves are superposed. The speed of the drop will affect, however on the time of impact. The higher the speed, the less time to impact the tablet. Hence, when impacting the tablet the drop will be larger if impacting at higher speed.

Time Evolution of the Shell Thickness as a Function of Initial Droplet Speed
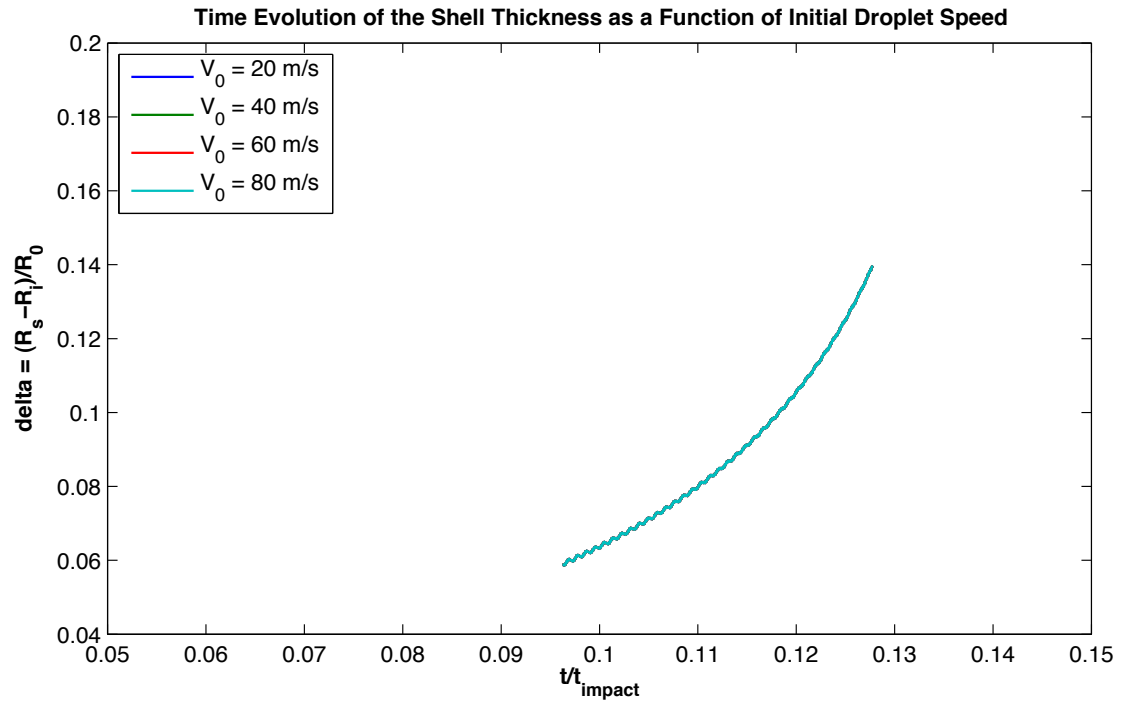
Figure 4.14: Temporal variation of the shell thickness as a function of the initial absolute drop speed

On the one side, a larger drop means less chances to have a shell formed or thinner shell sizes when impacting. But on the other size, larger drops means poorer coating, more splashing and splatting, more chances to obtain a porous and non-uniform coating.

4.4.5 Effect of Saturation Point

The saturation point refers to the mass fraction of solute at which a solution is considered saturated, meaning that if more solute is added it will not dissolve in the solvent, but it will precipitate. For the drops under study, a small saturation mass fraction implies an early saturation, which translates into an early formation of a shell. This, indeed, can be shown in figure 4.15, As the saturation mass fraction is increased, the drop begins forming a shell at later times.

However, what is remarkable is that all the curves have a very similar shape and slope, meaning that $Y_{s,sat}$ has very little effect on the drop vaporization and shell

formation, and has greater effect on the time at which the shell begins to form.
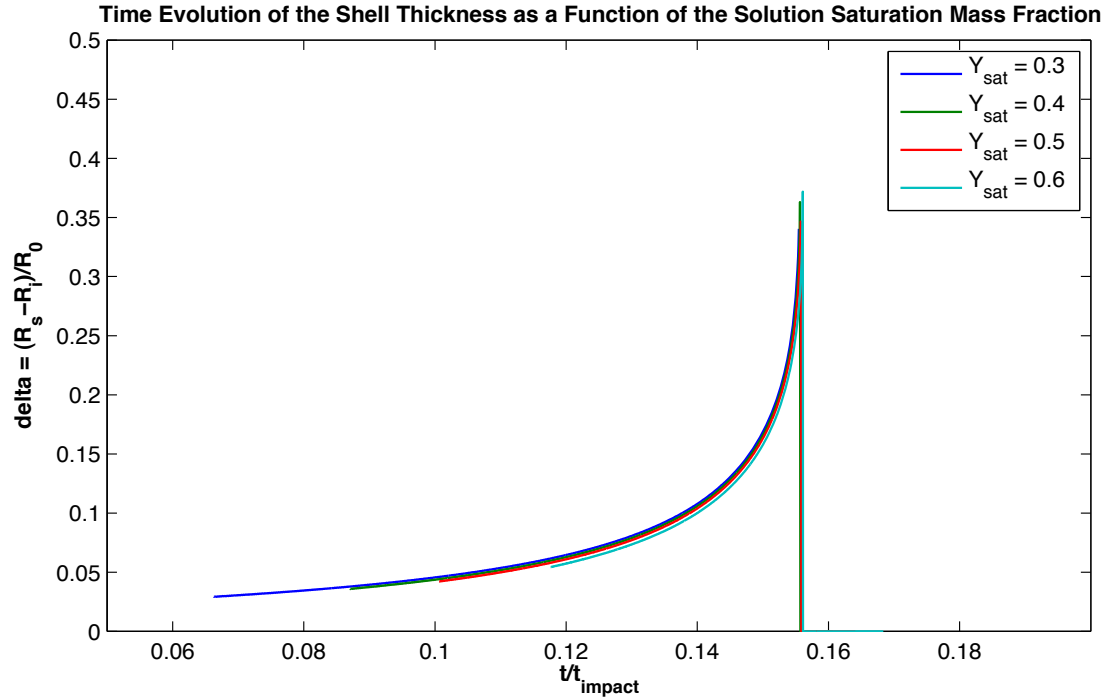

Figure 4.15: Temporal variation of the shell thickness as a function of the solute saturation mass fraction

The next figure 4.16, is a detailed view of the beginning of the shell formation. As already mentioned before, larger saturation mass fractions translate into larger times to reach saturation. However, in this figure we can also observe that smaller saturation mass fractions induce slightly larger shell thicknesses. A drop with smaller saturation mass fraction, such as $Y_{s,sat} = 0.3$, means a larger mass fraction of precipitate solute and solvent, but since the solvent vaporizes at its own rate at the surface, more precipitation must be occurring, hence, these drops form thicker shells. However, the increase is very small because the solute precipitation is not solely controlled by the saturation mass fraction, but also by the solvent vaporization.

This last figure 4.17 shows a detailed view of later stages of vaporization and shell formation. In here, it is observed that at approximately $t/t_{impact} = 0.155$, the plot shows a peak, a maximum and then a sudden decrease. This part of the plot is calculated by the program but has no physical meaning, and was included to raise the questions of when is the program giving physical solutions and when should it
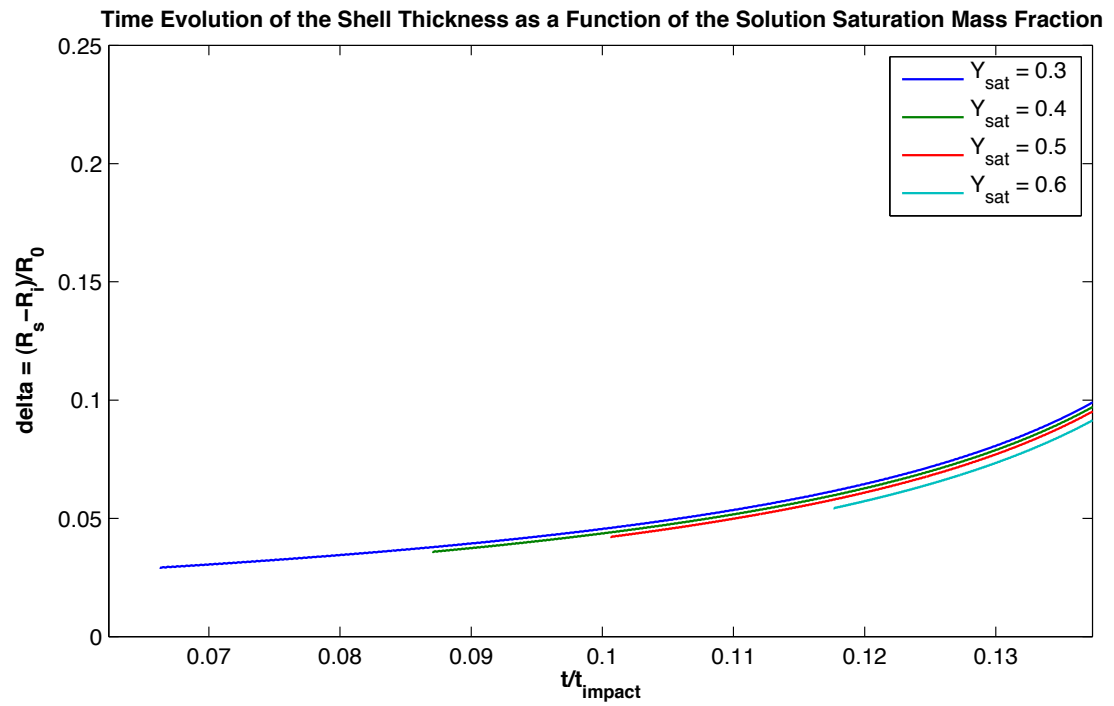
Figure 4.16: Detail view of the early stages of the shell formation. Smaller saturation fractions provide earlier shell formation

Time Evolution of the Shell Thickness as a Function of the Solution Saturation Mass Fraction
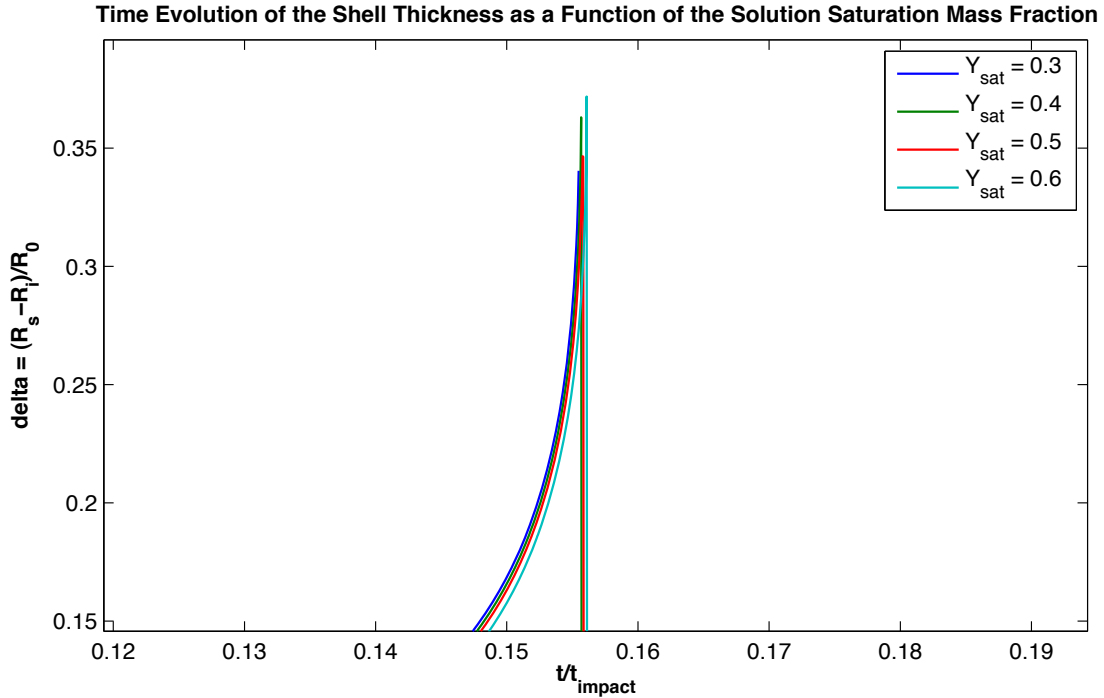
Figure 4.17: Detail of the late stages of the shell formation. Failure of the program to predict the shell thickness

stop calculating.

The peak and sudden decrease is due to the interaction of two variables, the saturation mass fraction and the maximum packing (volume fraction). Recalling the equation 3.36 from chapter 3, the linear combination $\alpha_m + Y_{s,sat}\frac{\rho_{solv}}{4\pi\rho_s}$ is present. Therefore, there will be a set of $Y_{s,sat}$ and α_m for which this subtraction may be zero or negative, inducing non physical solutions for the inner radius.

This means that there are certain combinations of $Y_{s,sat}$ and α_m that our model cannot resolve after reaching a certain drop size and shell thickness. However, we believe that most of these combinations are also non physical after a certain drop and shell size. We have to recall again that the maximum packing is the maximum volume fraction at which the precipitate can be compacted, while the saturation point is the maximum mass fraction of solute dissolved in a drop, so there is an indirect relationship between them. The droplet may be too small and the shell too thick to continue precipitating. However, there is still dissolved solute that may potentially precipitate.

Using mass and heat transfer equations within the drop, taking into account the diffusion process even after the drop is maximally packed, as well as a more realistic model for the precipitation process might resolve this problem. In reality, the solute precipitates in form of fibers, which have a very different behavior than spherical particles. Although the volume fraction can be represented as its equivalent spherical volume fraction, the underlying fiber physics may not be similar to spherical particles physics. However, for the purpose of this project, the model has shown to be accurate enough, capturing most of the physical phenomena occurring within the droplet.

4.4.6   Effect of Maximum Packing α_m

Define α_m the packing density of a packing of spheres, to be the fraction of a volume filled by the spheres. In three dimensions, there are three periodic packings for identical spheres: cubic lattice, face-centered cubic lattice, and hexagonal lattice. It was hypothesized by Kepler in 1611 that close packing (cubic or hexagonal, which have equivalent packing densities) is the densest possible, and this assertion is known as the Kepler conjecture.In this particular problem, the maximum packing α_m is the maximum volume fraction at which the precipitate can be compacted. The higher this number is, the more compacted the precipitate can be, which means the thinner the shell will be. However, it is not a variable of the problem, it is intrinsec to the problem.

Many experimental, analytical and numerical studies (summary in [59]) have been done to solve the problem of the maximum packing volume fraction to compact spheres, in random order or in lattices. The packing densities for several types of sphere packings range from 0.34 to 0.74, while this packing number for randomly packed spheres is between 0.51 and 0.64.

In figure 4.18 α_m ranges from 0.4 to 0.55. The plot shows a tremendous decrease on the slope of the temporal evolution of the shell thickness as the maximum packing is increased. However, as mentioned for the previous parameter study, certain values of α_m and $Y_{s,sat}$ are not physical once a certain drop and shell size are reached. But, despite these non-physical time ranges, the tendency of the shell growth slowing

Shell Thickness as a Function of the Maximum Packing of Precipitating Solid Particles
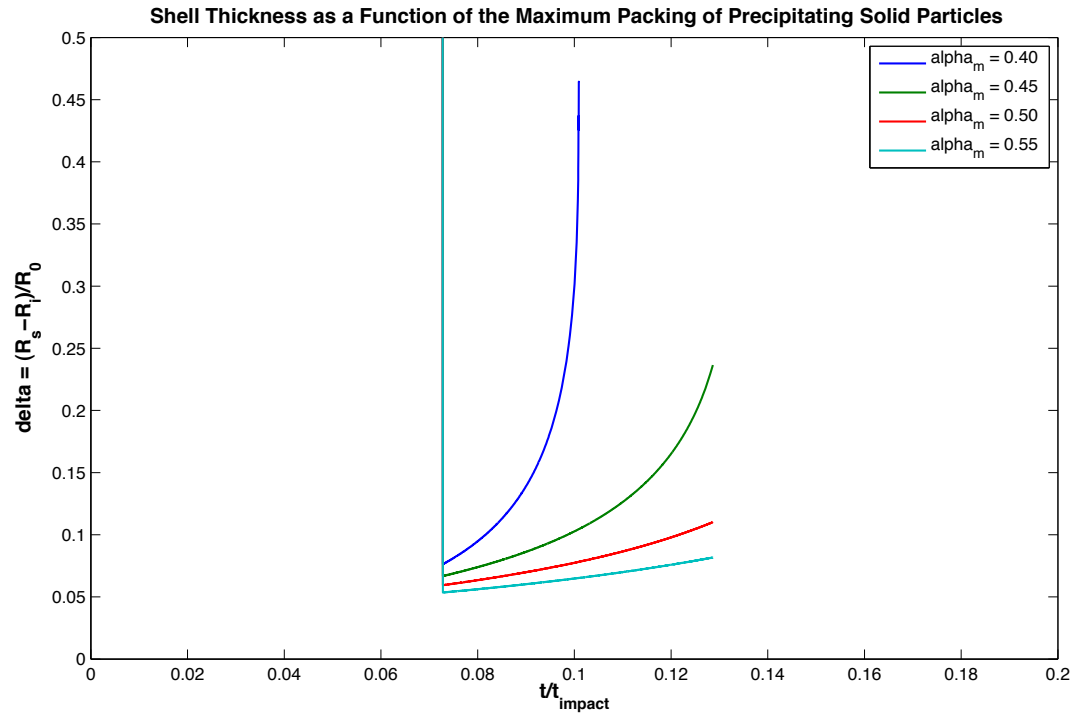

Figure 4.18: Temporal variation of the shell thickness as a function of maximum packing at the shell

down as the α_m increases is clear.

Chapter 5

Conclusions

5.1   Summary

The main goal during this project was the development of two simplified mathematical models that would capture the main physics of the vaporization process of droplets of solutions and suspensions coatings used in the pharmaceutical industry, as the spray travels from the atomizer until reaching the bed of tablets. As a result of this study, we were able to develop a graphical user interface program (using MatLab) that can be used during the preliminary lab testing of different coating processes. This program allows the user to vary the coating solution composition, drying air and atomization parameters, as well as coating device (through the distance to tablet parameter).

We have developed simplified models for the vaporization of droplets of coating solutions and suspensions, immersed in a turbulent jet of air. These models provide tools to predict spatial and temporal composition and size of the droplets prior to impacting the bed of tablets. For the case of solution coatings, we are able to predict whether or not a fully packed shell will form at the surface of the droplet during the coating process, as the drop travels to impact the tablet; as well as predict the time at which this shell is formed.

A parametric study was also performed for both models, and we have quantified the parameters that will affect more drastically the drop composition and its vaporization process. As stated in chapter 1, this parametric study as well as the

models will allow to ponder which are potential control and optimization parameters to take into account to improve the design and efficiency of the coating process.

5.2   Possible Future Work

As mentioned in the previous chapters, the models developed in this project have assumptions and simplifications embedded on them. We have then studied an overly idealized problem. All of the simplifications have been checked and therefore justified. However, although these are correct assumptions in an idealized problem, they may not capture all of the physics phenomena occurring during the coating process.

This is an intricate problem where many physics disciplines are needed to describe the complete process: thermodynamics, heat and mass transfer, systems dynamics, fluid mechanics. Physics modeling consist of obtaining a simplified analytical model that can describe fairly well a complex process.

However, there is still room for improvement in the models here explained. An ambient with some initial concentration of the solvent's vapor can be included in the model, which would most likely slower the vaporization process, reaching a vapor saturated equilibrium at the drop surface at an early stage of the vaporization. A drying air temperature gradient, having a maximum temperature at the drying air injection points and decreasing as it gets mixed with the atomization air, which is at room temperature, may induce as well a decrease in the drop vaporization and shell growth. As for the initial conditions used in the MatLab program, instead of the turbulent air jet centerline speed, a fully developed turbulent spray jet (including drop to drop interaction) may be included in the overall actual coating process model.

References

[1] T. Halamus, P. Wojciechowski, and I. Bobowska, "Synthesis and characterization of (hydroxypropyl)cellulose/tio2 nanocomposite films," *Polymers for Advances Technologies*, vol. 19, pp. 807–811, 2008.

[2] S. A. Altinkaya and B. Ozbas, "Modeling of asymmetric membrane formation by dry-casting method," *Journal of Membrane Science*, vol. 230, pp. 71–89, 2004.

[3] S. A. Altinkaya and H. Yenal, "In vitro drug release rates from asymmetric-membrane tablet coatings: Prediction of phase-inversion dynamics," *Biochemical Engineering Journal*, vol. 28, pp. 131–139, 2006.

[4] Y. H. Kim, Y. H. Bae, and S. W. Kim, "ph/temperature-sensitive polymers for maceomolecular drug loading and release," *Journal of Controlled Release*, vol. 28, pp. 143–152, 1994.

[5] G. P. Denisova, T. P. Ustinova, E. G. Povolotskii, S. V. Igonina, and N. Y. Martynova, "Effect of the structure of cellulose acetate solutions on the morphological characteristics of ultrafiltration membranes," *Fibre Chemistry*, vol. 34, no. 5, pp. 335–337, 2002.

[6] Y. A. Kostrov, M. Y. Ivan, Z. V. Baibakova, V. M. Golubev, and L. P. Perepechkin, "The molecular weight and fractional composition of the cellulose acetate as factors in the properties of acetate fibre," *Khimicheskie Volokna*, vol. 1, pp. 44–46, 1973.

[7] C. K. Law, "Recent advances in droplet vaporization and combustion," *Prog. Energy Combustion Science*, vol. 8, pp. 171–201, 1982.

[8] Y. Solomon and B. Natan, "Experimental investigation of the combustion of organic-gellant-based gel fuel droplets," *Combustion Science and Technology*, vol. 178, pp. 1185–1199, 2006.

[9] R. Crawley, "A hollow droplet generator for polymer shell production," *Journal of Vacuum Science Technology*, vol. 4, no. 3, pp. 1138–1141, 1986.

[10] H. Zhuang, P. Lu, S. P. Lim, and H. P. Le, "Study of the evaporation of colloidal suspension droplets with the quartz crystal microbalance," *Langmuir*, vol. 24, pp. 8373–8378, 2008.

[11] J. C. Lasheras, E. Villermaux, and E. J. Hopfinger, "Break-up and atomization of a round water jet by a high-speed annular air jet," *Journal of Fluid Mechanics*, vol. 357, pp. 351–379, 1998.

[12] J. C. Lasheras and E. J. Hopfinger, "Liquid jet instability and atomization in a coaxial gas stream," *Annual Review of Fluid Mechanics*, vol. 32, pp. 275–308, 2000.

[13] C. M. Varga, J. C. Lasheras, and E. J. Hopfinger, "Initial breakup of a small-diameter liquid jet by a high-speed gas stream," *Journal of Fluid Mechanics*, vol. 497, pp. 405–434, 2003.

[14] A. Mansour and N. Chigier, "Air-blast atomization of non-newtonian liquids," *J. Non-Newtonian Fluid. Mech.*, vol. 58, pp. 161–194, 1995.

[15] E. J. Hopfinger and J. C. Lasheras, "Explosive breakup of a liquid jet by a swirling coaxial gas jet," *Physics of Fluids*, vol. 8, no. 7, pp. 1696–1698, 1996.

[16] A. Aliseda, "Atomization of viscous and non-newtonian liquids by a coaxial, high speed gas jet. experiments and droplet size modeling," *International Journal of Multiphase Flow*, vol. 34, pp. 161–175, 2008.

[17] P. Antaki and F. A. Williams, "Observations on the combustion of boron slurry droplets in air," *Combustion and Flame*, vol. 67, pp. 1–8, 1987.

[18] S. Nesic and J. Vodnik, "Kinetics of droplet evaporation," *Chemical Engineering Science*, vol. 46, no. 2, pp. 527–537, 1991.

[19] W. A. Sirignano, *Fluid Dynamics and Transport of Droplets and Sprays*, ch. 2. Theory of Isolated Droplet Vaporization, Heating and Acceleration. Cambridge University Press, 1999.

[20] W. A. Sirignano, "Fuel droplet vaporization and spray combustion theory," *Prog. Energy Combustion Science*, vol. 9, pp. 291–322, 1983.

[21] C. K. Law, C. H. Lee, and N. Srinivasan, "Combustion characteristics of water-in-oil emulsion droplets," *Combustion and Flame*, vol. 37, pp. 125–143, 1980.

[22] A. L. Yarin, G. Brenn, and O. Kastner, "Evaporation of acoustically levitated droplets," *Journal of Fluid Mechanics*, vol. 399, pp. 151–204, 1999.

[23] F. R. Newbold and N. R. Amundson, "A model for evaporation of a multicomponent droplet," *AIChE Journal*, vol. 19, no. 1, pp. 22–30, 1973.

[24] C. K. Law, "Multicomponent droplet combustion with rapid internal mixing," *Combustion and Flame*, vol. 26, pp. 219–233, 1976.

[25] M. Renksizbulut and M. Bussmann, "Multicomponent droplet evaporation at intermediate reynolds numbers," *International Journal of Mass Transfer*, vol. 36, no. 11, pp. 2827–2835, 1993.

[26] W. A. Sirignano, *Fluid Dynamics and Transport of Droplets and Sprays*, ch. 3. Multicomponent Liquid Droplets. Cambridge University Press, 1999.

[27] S. R. L. Werner, R. L. Edmods, J. R. Jones, J. E. Bronlund, and A. H. J. Paterson, "Single droplet drying: Transition from the effective diffusion model to a modified receding interface model," *Powder Technology*, vol. 179, pp. 184–189, 2008.

[28] S. R. L. Werner, R. L. Edmonds, and J. R. Jones, "Single droplet drying. 2. maltodextrin de5 drying kinetics and mathematical model validation." submitted for publication.

[29] M. Mezhericher, A. Levy, and I. Borde, "Theoretical drying model of single droplets containing insoluble or dissolved solids," *Drying Technologies*, vol. 25, pp. 1035–1042, 2007.

[30] N. Dalmaz, H. O. Ozbelge, A. N. Eraslan, and Y. Uludag, "Heat and mass tranfer mechanisms in drying of a suspension droplet: A new computational model," *Drying Technology*, vol. 25, no. 2, pp. 391–400, 2007.

[31] A. L. Yarin, G. Brenn, and O. Kastner, "Drying of acoustically levitated droplets of liquid–solid suspensions: Evaporation and crust formation," *Physics of Fluids*, vol. 14, no. 7, pp. 2289–2298, 2002.

[32] M. Eslamian, M. Ahmed, and N. Ashgriz, "Modeling of solution droplet evaporation and particle evolution in droplet-to-particle spray methods," *Drying Technology*, vol. 27, pp. 3–13, 2009.

[33] M. D. Haw, M. Gillie, and W. C. K. Poon, "Effect of phase behavior on the drying of colloidal suspensions," *Langmuir*, vol. 18, pp. 1626–1633, 2002.

[34] F. Parisse and C. Allain, "Drying of colloidal suspension droplets: Experimental study and profile renormalization," *Langmuir*, vol. 13, 3598-3602 1997.

[35] The Royal Society, *Time-dependent geometrical changes in a ceramic ink droplet*, vol. 458, Mathematical, Physical and Engineering Sciences, 2002.

[36] L. Pauchard and C. Allain, "Buckling instability induced by polymer solution drying," *Europhysics Letters*, vol. 62, no. 6, pp. 897–903, 2003.

[37] C. T. Avedisian, "An experimental study of high-pressure bubble growth within multicomponent liquid droplets levitated in a flowing stream of another immiscible liquid," in *Series A. Mathematical and Physical Sciences*, vol. 409, pp. 271–285, The Royal Society, 1987.

[38] M. Eslamian and N. Ashgriz, "Evaporation and evolution of suspended solution droplets at atmospheric and reduced pressures," *Drying Technology*, vol. 25, pp. 1009–1020, 2007.

[39] M. Rein, "Phenomena of liquid drop impact on solid and liquid surfaces," *Fluid Dynamics Research*, vol. 12, pp. 61–93, 1993.

[40] A. Yarin, "Drop impact dynamics: Splashing, spreading, receding, bouncing...," *Annual Review of Fluid Mechanics*, vol. 38, pp. 159–192, 2006.

[41] D. A. Bolleddula, A. Berchielli, and A. Aliseda, "Impact of a heterogeneous liquid droplet on a dry surface: Application to the pharmaceutical industry," *Advances in Colloid and Interface Science*, 2010.

[42] A. Asai, M. Shioya, S. Hirasawa, and T. Okazaki, "Impact of an ink drop on paper," *Journal of imaging science and technology*, vol. 37, 1993.

[43] T. Mao, D. Kuhn, and H. Tran, "Spread and rebound of liquid droplets upon impact on flat surfaces," *AIChE Journal*, vol. 43, pp. 2169–2179, 1997.

[44] A. Liñán, "Conducción de calor en sólidos." lecture notes from Escuela Técnica Superior de Ingenieros Aeronáuticos, June 2005.

[45] F. A. Williams, "Ignition and burning of single liquid droplets," *Acta Astronautica*, vol. 12, no. 7/8, pp. 547–443, 1985.

[46] A. Liñán, "Theory of droplet vaporization and combustion." lecture notes from Universidad Politécnica de Madrid, 1985.

[47] S. M. Frolov, F. S. Frolow, and B. Basara, "Simple model of transient drop vaporization," *Journal of Russian Laser Russian Research*, vol. 27, no. 6, pp. 562–574, 2006.

[48] P. Antaki and F. A. Williams, "Transient processes in a nonrigid slurry droplet during liquid vaporization and combustion," *Combustion Science and Technology*, vol. 49, no. 5-6, pp. 289–296, 1986.

[49] E. J. Hinch, "Hydrodynamics at low reynolds number: A bried and elementary introduction," *Disorder and Mixing*, vol. 152, pp. 43–55, 1988.

[50] G. K. Batchelor, "Developments in microhydrodynamics," *Theoretical and Applied Mechanics*, 1976.

[51] E. M. Purcell, *Physics and Our World: A Symposium in Honor of Victor F. Weisskopf*, ch. Life at Low Reynolds Number. American Institute of Physics, 1976.

[52] E. Ferdman, M. V. Otügen, and S. Kim, "Effect of initial velocity profile on the development of round jets," *Journal of Propulsion and Powe*, vol. 16, no. 4, pp. 676–686, 2000.

[53] M. Rodríguez, "Introducción a la capa límite turbulenta bidimensional e incompresible." lecture notes from Escuela Técnica Superior de Ingenieros Aeronáuticos.

[54] H. Schlichting, *Mc Graw Hill Series in Mechanical Engineering. Boundary Layer Theory*. Mc Graw Hill, 1955.

[55] F. M. White, *Mc Graw Hill Series in Mechanical Engineering. Viscous Fluid Flow*. Mc Graw Hill, 1991.

[56] P. Burattini, R. A. Antonia, and L. Danalia, "Similarity in the far field of a turbulent round jet," *Physics of Fluids*, vol. 17, no. 1-14, 2005.

[57] M. N. Lotfollahi, R. D. Salehi, and H. Modarress, "Ternary phase diagram for polymer/solvent/supercritical-co2," *Iranian Journal of Chemical Engineering*, vol. 3, no. 2, pp. 64–72, 2006.

[58] P. van de Witte, P. J. Dijkstra, J. W. A. van den Berg, and J. Feijen, "Phase separation processes in polymer solutions in relation to membrane formation," *Journal of Membrane Science*, vol. 117, pp. 1–31, 1996.

[59] E. W. Weisstein, "Sphere packing," 2010.